

1 **Ocean acidification enhances primary productivity and**
2 **nocturnal carbonate dissolution in intertidal rock pools**

3

4 **Narimane Dorey^{1,†}, Sophie Martin^{2,3}, Lester Kwiatkowski⁴**

5

6 ¹ LMD-IPSL, CNRS, École Normale Supérieure/PSL Res. Univ, École Polytechnique, Sorbonne
7 Université, Paris, 75005, France

8 ² CNRS, UMR7144, Station Biologique, Place Georges Teissier, 29688 Roscoff Cedex, France

9 ³ Laboratoire Adaptation et Diversité en Milieu Marin, Sorbonne Universités, UPMC Univ Paris
10 06, Station Biologique, Place Georges Teissier, 29688 Roscoff Cedex, France

11 ⁴ LOCEAN Laboratory, Sorbonne Université-CNRS-IRD-MNHN, Paris, 75005, France

12

13 † Correspondence to: Narimane Dorey

14 École Normale Supérieure,
15 Département de Géosciences,
16 24 rue Lhomond, 75005 Paris, France

17 E-mail: narimane.dorey@gmail.com

18

19 **ABSTRACT**

20 Human CO₂ emissions are modifying ocean carbonate chemistry, causing ocean acidification, and
21 likely already impacting marine ecosystems. In particular, there is concern that coastal, benthic
22 calcifying organisms will be negatively affected by ocean acidification, a hypothesis largely
23 supported by laboratory studies. The inter-relationships between carbonate chemistry and marine
24 calcifying communities *in situ* are complex and natural mesocosms such as tidal pools can provide
25 useful community-level insights. In this study, we manipulated the carbonate chemistry of
26 intertidal pools to investigate the influence of future ocean acidification on net community
27 production (NCP) and calcification (NCC) at emersion. Adding CO₂ at the start of the tidal
28 emersion to simulate future acidification (+1500 μatm pCO₂, target pH: 7.5) modified net
29 production and calcification rates in the pools. By day, pools were fertilized by the increased CO₂
30 (+20 % increase in NCP, from 10 to 12 mmol O₂ m⁻² hr⁻¹), while there was no measurable impact
31 on NCC. During the night, pools experienced net community dissolution (NCC < 0), even in
32 present-day conditions, when waters were supersaturated with regards to aragonite. Adding CO₂
33 in the pools increased nocturnal dissolution rates by 40% (from -0.7 to -1.0 mmol CaCO₃ m⁻² hr⁻¹)
34 with no consistent impact on night community respiration. Our results suggest that ocean
35 acidification is likely to alter temperate intertidal community metabolism on sub-daily timescales,
36 enhancing both diurnal community production and nocturnal calcium carbonate dissolution.

37 **SHORT SUMMARY**

38 Human CO₂ emissions are modifying ocean carbonate chemistry, causing ocean acidification, and
39 likely already impacting marine ecosystems. Here, we added CO₂ in intertidal pools at the start of
40 emersion to investigate the influence of future ocean acidification on net community production
41 (NCP) and calcification (NCC). By day, adding CO₂ fertilized the pools (+20 % NCP). By night,
42 pools experienced net community dissolution, a dissolution that was further increased (+40 %) by
43 the CO₂ addition.

44 **Keywords:** Ocean acidification, calcification, coralline algae, mesocosms, primary production,
45 temperate community, tidal pool

46 INTRODUCTION

47 The ongoing increase of anthropogenic carbon dioxide (CO₂) in the atmosphere and the ocean –
48 resulting in ocean acidification - is likely to create adverse living conditions for marine coastal
49 communities (IPCC, 2019). Ocean acidification is projected to further decrease average surface
50 pH by up to 0.4 units by 2100 (scenario RCP8.5, Kwiatkowski et al., 2020), and is identified as a
51 major threat to marine ecosystems (IPCC, 2019). Lower seawater pH has significant effects on
52 marine organisms physiology and fitness: from altered survival and reduced growth (see review
53 by Kroeker et al. 2013), to changes in pH homeostasis (e.g., Kottmeier et al., 2022), metabolic
54 rates, and energy trade-offs (e.g., Dorey et al., 2013; Pan et al., 2015) and reduced feeding
55 efficiency (e.g., Stumpp et al., 2013). Marine calcifiers - the builders of calcified structures
56 (CaCO₃) - have been a focus of ocean acidification research due to the sensitivity of calcification
57 to the carbonate saturation state (Ω), defined as follows:

$$58 \quad \Omega = [\text{Ca}^{2+}] [\text{CO}_3^{2-}] / K'_{\text{sp}}$$

59 where K'_{sp} is the stoichiometric solubility product for the considered carbonate polymorph (i.e.,
60 Ω_{a} for aragonite or Ω_{c} for calcite). The saturation state depends on temperature, pH, and pressure
61 (lower Ω when pH or temperature decreases and pressure increases). When $\Omega < 1$, inert carbonate
62 minerals tend to dissolve. The polymorphs composing the calcified structure like calcite and to a
63 greater extent aragonite and high-magnesium calcite, are prone to dissolution when pH decreases.
64 For instance, in Atlantic surface waters (at 20°C), saturation state equilibrium ($\Omega = 1$) is reached
65 at pH 7.3 ($p\text{CO}_2 = 2650 \mu\text{atm}$) for calcite but at pH 7.6 (1250 μatm) for aragonite. For high-
66 magnesium calcite, experiments from (Yamamoto et al., 2012) demonstrate that inert (dead) high-
67 magnesium calcite from coralline algae passively dissolves at Ω_{a} values between 3.0 and 3.2 (also
68 see Ries et al. 2016). Organisms with calcified structures are thus likely to experience reduced net
69 calcification due to ocean acidification, both through enhanced dissolution, and reduced gross
70 calcification rates.

71 Aside from acidifying the ocean (increased H⁺), increased ocean CO₂ uptake could affect
72 the productivity of algae and marine plants. As CO₂ dissolves in the ocean, the dissolved inorganic
73 carbon (DIC: CO₂, HCO₃⁻ and CO₃²⁻) concentration increases. DIC is the substrate for marine
74 photosynthesis (mainly CO₂ and HCO₃⁻), and as such, it can limit photosynthetic rates when scarce.

75 In algae and marine plants that are carbon limited (permanently or periodically), elevated DIC
76 could also directly increase photosynthetic rates and Mackey et al., (2015) propose that these rates
77 could be further increased by the higher concentration gradient between water and the
78 photosynthetic cells. However, the authors point out that while positive effects are theoretically
79 expected, they may be small, specific to species' biology and the environment they live in, and
80 difficult to predict (see also Hurd et al., 2019). In terrestrial ecosystems, the Intergovernmental
81 Panel on Climate Change defines CO₂ fertilization as 'the enhancement of plant growth as a result
82 of increased atmospheric CO₂ concentration' (Jia et al., 2019) and reports that CO₂ fertilization
83 has likely already happened, although the magnitude of this effect depends on the plants, or
84 assemblages/ecosystems considered (and on other factors constraining growth).

85 The response of single species to changes such as ocean acidification and increased DIC
86 concentrations are often insufficient to predict community-level impacts. Ecological interactions
87 such as competition or predation can affect the outcome of perturbation experiments (Kroeker et
88 al., 2012). For instance, Paiva et al. (2021) showed that the laboratory growth of an isopod species
89 was an order of magnitude slower than when raised in the presence of other species from its
90 community. In another study, Legrand et al. (2019) showed that the presence of grazers increased
91 coralline algal calcification (+50% in winter and +100% in summer), but when grazers were
92 combined with ocean acidification, algal calcification decreased more than with acidification
93 alone. Not taking into account such interactions can therefore result in poorly characterizing the
94 effects of ocean acidification. Furthermore, while critical for a mechanistic understanding of the
95 processes affecting marine biota, laboratory studies are seldom realistic. Typically performed in
96 controlled, simplified, and stable conditions (e.g., with respect to temperature and food), laboratory
97 studies can better assess the effect of pH alone (Widdicombe et al., 2010). However exposure to a
98 stable pH (e.g., 7.6 vs. 8.0), fails to reflect the daily and seasonal variability observed in natural
99 ecosystems, in particular coastal ones (Torres et al., 2021). Natural mesocosm perturbation
100 experiments are thus essential tools to investigate future changes in variable and complex
101 ecosystems, difficult to capture in the lab (Barry et al., 2010; Andersson et al., 2015).

102 Most *in situ* mesocosm experiments investigating the effect of ocean acidification have
103 been conducted on planktonic communities, kept in large "bags" equilibrated to the desired pH
104 (Riebesell et al., 2013). These studies demonstrate that adding CO₂ can significantly change the

105 organization of the plankton community (Spisla et al., 2021), and increase autotrophic biomass in
106 high-nutrient conditions (Schulz et al., 2013). Due to the technical challenges, however, benthic
107 calcifying communities are seldom manipulated this way *in situ* (Widdicombe et al., 2010). Two
108 such manipulation experiments are the studies by Albright et al. (2016, 2018), where the authors
109 used NaOH and CO₂ to reproduce pre-industrial and future pH conditions on a coral reef and found
110 evidence that reef growth had been reduced by 7% over the industrial era and was likely to decline
111 further. Other studies have investigated such community-level effects by either simulating
112 “artificial”, simpler, assemblages in laboratory setups (e.g., Cox et al., 2015; Pansch et al., 2016)
113 or using phenomena such as natural CO₂ vents. For instance, in the vents of Ischia, as pH decreases,
114 the presence of calcifying species declines (see review by Foo et al., 2018). Alternatively,
115 Kwiatkowski et al. (2016) used locally-induced acidification due to respiration (no CO₂ addition)
116 in tidal pools, a naturally closed system, and demonstrated that nighttime dissolution of these
117 communities was positively correlated with Ω . Here, we used tidal pools of the English Chanel as
118 ephemeral mesocosms, where we modified carbonate chemistry conditions at the start of emersion
119 through CO₂ addition.

120 Temperate rocky tidal pools - or rockpools - are highly dynamic systems that have been long
121 studied by naturalists since they are easy to reach and their ecosystem structure generally resemble
122 subtidal benthic communities (Ganning, 1971). Tidal pool organisms from the upper shore, well-
123 adapted to pool conditions, form typical benthic communities: often low in diversity, they consist
124 of a few characteristic macroalgal (e.g., *Ulva sp.*) and animal species (e.g., limpets). In winter, red
125 macroalgae – including calcifying algae – often dominate the pools and while they do not disappear
126 in summer, a bloom of soft green macroalgae is generally observed during the warm season.
127 Temperature, salinity, oxygen, and pH in the pools are extremely variable, often far outside the
128 seasonal range of nearby free-flowing seawater (Legrand et al., 2018a; Morris and Taylor, 1983).
129 Tidal pools generally emerge from the ocean twice a day in regions of semidiurnal tides with the
130 duration dependent on shore location and the tidal coefficient. On short timescales tidal pools act
131 as closed systems, with carbonate chemistry easily manipulated and temporal changes reflecting
132 *in situ* community metabolism (no water mass transport and negligible air-sea gas exchange).

133 In the present study, we used tidal pools as natural mesocosms to investigate the effect of ocean
134 acidification on communities dominated by calcifying red algae. We measured diurnal and

135 nocturnal net community calcification and production (or respiration) following CO₂ addition
136 across three seasons (winter, spring, and summer), to assess how tidal pool community metabolism
137 may respond to end of the 21st century high ocean acidification (pH 7.5).

138

139 **MATERIAL AND METHODS**

140 **Field site**

141 The experiments were performed on a rocky intertidal shore characterized by granitic substrate on
142 the North coast of Brittany, France, between 2019 and 2021. The beach of Bloscon (48°43'30.0"N
143 3°58'10.5"W) is situated in Roscoff at the entrance of the Bay of Morlaix and has a hydrology
144 principally affected by the waters of the English Channel and to a lesser extent the Penzé and
145 Morlaix rivers (**Fig. 1**). This area is characterized by strong, oscillating, semidiurnal tides of up to
146 9 m. Temperatures are generally low in the deeper flowing water (from 9-10 °C in winter to 16-17
147 °C in summer), and salinity is close to that of the adjacent Atlantic (~35; see **Supp. Mat. Fig. S1**
148 for detailed temperature and salinity data from the two nearby SOMLIT monitoring stations
149 Estacade and Astan, a network described in Cocquempot et al., 2019).

150 **Tidal pool characterization**

151 For this study, we chose five tidal pools with high coverage in calcifying algae ($\geq 30\%$ of the pool
152 surface area). Both crustose (CCA) and articulated (branching) coralline algae (ACA) were
153 present. The field site has an eastern exposure, resulting in full morning sun and relatively early
154 shade in the evening. Foreshore locations of the pools resulted in daily emersion year-round
155 including during neap tides (mid-tide, approx. 5-6 m above chart datum). Pools emerged for 6-7 h
156 during low-tide periods. During that time, pools were completely separated from the adjacent open
157 water and their depths were effectively constant in winter (low-evaporation season), an indication
158 that there was no seawater leakage.

159 The volume of each of the five pools (from 16 to 39 L; **Fig. 2**) was estimated in April 2021
160 at the end of the emersion period just before high-tide flooding, by measuring salinity changes
161 when a known volume of freshwater was added and well mixed. To estimate the pools' initial
162 volumes, we also took into consideration the measured salinity changes throughout the emersion

163 period to estimate evaporative losses and combined this with the volume directly lost through
164 water sampling (see below). The pool projected area and the relative area covered by each type of
165 algae were estimated from aerial photographs, with a scale and analyzed using ImageJ (U. S.
166 National Institutes of Health, Bethesda, Maryland, USA, <https://imagej.nih.gov/ij>). Pool area
167 ranged from 0.3 to 0.7 m² (**Fig. 2**). The pools had slightly different community composition with
168 dominant calcifying red algae represented by *Lithophyllum incrustans* (CCA: 30 to 77 % of the
169 benthic cover) and *Ellisolandia elongata* (ACA: 0 to 6 % of the benthic cover). The remaining
170 pool area was either free of algal cover with only bare granitic rock visible or covered by soft
171 macroalgae. In summer (September 2020 and 2021), the pools also hosted the green algae *Ulva*
172 *sp.* and *Enteromorpha sp.* (2 to 44 % of the benthic cover: see **Supp. Mat. Pools: Fig. SP1-2**, for
173 results detailed by season) and, in Pool E, small single branches of the brown algae *Sargassum*
174 *muticum*, covering less than 0.5 % of the pool. One limit of this method of aerial photography is
175 that it only takes into account what is visible from above (2D). These estimates may thus be biased
176 against algae that were hidden under the green algae canopy in summer or that were in
177 crevices/under rocks. We also noted the presence of diverse heterotrophs such as anemones, sea
178 sponges, small gobies, and shrimps. Calcifying invertebrates were represented by four gastropod
179 species: *Phorcus lineatus*, *Patella ulyssiponensis*, *Patella vulgata* and *Gibbula pennanti*.

180 **Study design and seawater manipulation**

181 Fieldwork was conducted during the low-tide emersion periods, day and night. We refer to the
182 period from the beginning to the end of the pool emersion as a “low-tide emersion period” and to
183 each seasonal sampling period as a “field session” (**Table 1**). We sampled during three seasons:
184 winter (February 2020 and 2021), spring (April 2021), and summer (September 2020 and 2021).
185 During each field session, all the pools experienced both “future” (approximately year 2100 under
186 high emissions) and present-day (“present”, non-manipulated control) initial carbonate chemistry
187 conditions. During each low-tide emersion period (n = 23), we randomly selected two or three
188 pools in which we decreased pH to 7.5 at the start of the emersion. The following low-tide
189 emersion period, this was reversed and pools that had been subject to present-day conditions in the
190 previous low-tide emersion period were subject to future conditions and *vice versa*. However, due
191 to diverse constraints, in two of the 23 emersion periods all the pools were left under present-day
192 conditions.

193 **Table 1: Sampling schedule:** The dates of each field session are presented. Pools were monitored
 194 throughout multiple low-tide emersion periods (diurnal and nocturnal).

Season	Dates	Low-tide emersion periods (N)	
		Diurnal	Nocturnal
Winter	14-17 February 2020	2	0
	9-19 February 2021	8	2
Spring	28-29 April 2021	2	0
Summer	2-11 September 2020	5	1
	6-9 September 2021	0	3

195

196 In this experiment, we compared "present" and "future" seawater carbonate chemistry
 197 conditions. To simulate "future" carbonate chemistry conditions, we added small volumes of CO₂-
 198 enriched seawater (total of ~100-200 mL) at the start of the emersion period in 50 mL increments
 199 until the well-mixed pool water reached the desired pH levels (pH = 7.5, reached in less than 10
 200 min.). CO₂-enriched seawater was prepared by super-saturating adjacent seawater in CO₂ using a
 201 high-pressure CO₂ cylinder.

202 **Sampling and measurement of seawater parameters**

203 **Temperature, salinity, pH, oxygen, and ammonium:** From the start of the emersion period, we
 204 measured five parameters periodically using HACH-Lange (Loveland, USA) probes: temperature,
 205 pH_T (IntelliCAL PHC101, accuracy: ± 0.02 pH units), salinity (conductivity probe IntelliCAL
 206 CDC401, ± 0.1 units), oxygen concentration (optical sensor IntelliCAL LDO101, accuracy: ± 0.1
 207 mg L⁻¹ for 0 to 8 mg L⁻¹, ± 0.2 mg L⁻¹ for greater than 8 mg L⁻¹, maximum 22 mg L⁻¹) and NH₄⁺
 208 concentration (ion selective electrode IntelliCAL ISENH4181, range: 0.018 - 9000 mg L⁻¹ NH₄⁺-
 209 N). Pools were well-mixed before any measurement to assure no influence of gradients forming in
 210 the pools. The measurement frequency during the emersion periods was every 15-20 min during
 211 the day (n = 1392) and reduced to once an hour at night (n = 159), when temperature, pH and light
 212 variations were limited or absent. pH was calibrated on the total scale (pH_T) using TRIS (2-amino-
 213 2-hydroxy-1,3-propanediol) and AMP (2-aminopyridine) buffer solution with a salinity of 35.0,
 214 following the recommendations from (Dickson et al., 2007).

215 **Total alkalinity:** Discrete samples for total alkalinity (TA) analysis were collected hourly. The
216 average time between two samples was 1.0 ± 0.2 hours ($n = 492$, median = 1.0) during daytime
217 and 1.4 ± 0.9 hours ($n = 135$, median = 1.0) during nighttime. Seawater (150 mL) was filtered with
218 $0.7 \mu\text{m}$ GF/F borosilicates filters directly after sampling. These samples were stored in a dark cool
219 box until the end of the tide (max. 7 h). Upon return to the lab, they were stored at 4°C in the dark
220 until they were either analyzed within the week or poisoned with $50 \mu\text{L}$ of saturated HgCl_2 (see
221 "*sample processing*"). TA was assessed potentiometrically using 50.0 ± 0.5 g of seawater and a
222 semi-automated titration system (0.1 M HCl, Titrino 848 plus by Metrohm, Switzerland; electrode
223 calibrated on the National Bureau of Standards scale). TA was determined using Gran titration
224 (Gran, 1952) according to the method of Haraldsson et al. (1997) and verified against reference
225 standards provided by A. Dickson (Scripps Institute of Oceanography, University of South
226 California, San Diego, United States). TA samples were analyzed with single ($n = 312$) or duplicate
227 ($n = 320$) measurements (the median of the standard deviation between duplicates was $1.05 \mu\text{mol}$
228 kg^{-1}). TA was salinity-normalized before further calculations, to take into account possible dilution
229 from rain or concentration from evaporation.

230 To take into account the influence of the changes in nutrients (NO_3^- , NO_2^- , PO_4^{3-} and NH_4^+)
231 on the changes in TA (Gazeau et al., 2015), we sampled seawater for nutrients in winter (February
232 2020) and summer (September 2020). Samples were taken during the day at the start and end of
233 the emersion periods in the five pools. Around 60 mL of seawater was immediately filtered on 0.2
234 μm cellulose filters, stored in 125 mL polyethylene bottles in a cool dark box (max. 7h), and then
235 frozen at -20°C until analysis. Nutrient concentrations were obtained using an AA3 auto-analyzer
236 (Seal Analytical) using the method from Aminot & K  rouel (2007). Changes in nutrient
237 concentrations were near-negligible contributions to TA changes throughout a low-tide emersion
238 period ($< 6 \mu\text{mol kg}^{-1}$ i.e., $< 2\%$ of the observed change in TA, see full details in **Supp. Mat.**
239 **Nutrients**) and thus are ignored here.

240 **Light measurements:** Surface irradiance (photosynthetically active radiation, PAR) was
241 continuously recorded (every minute) during experiments at the field station, using a Li-Cor flat
242 quantum light sensor (LI-190R) and logger (LI-1500, LI-COR, Germany).

243 **Adjacent waters:** Temperature, salinity, pH and TA ($n = 5$) were similarly sampled and measured
244 at the sampling site during ebb tide, for the three seasons.

245 **Carbonate chemistry calculations**

246 The carbonate system parameters (e.g., $p\text{CO}_2$, DIC concentration, CO_3^{2-} concentration, and Ω_a , the
247 aragonite saturation state) were calculated from the measurements of pH_T , TA, temperature and
248 salinity using the R package *seacarb* (Gattuso et al., 2021) with the default dissociation constants
249 recommended by Dickson et al. (2007), except for the low temperatures encountered in February
250 2021 where the refined constants of Sulpis et al. (2020) were used. When salinity decreased by
251 more than 1.5 units per hour, data were excluded to avoid rain effects in the present study. When
252 calculated DIC and Ω_a were negative, likely due to inaccuracies in the measurement and
253 computation of the carbonate system, values were approximated to be 0 (7/627 values). The air-
254 sea gas fluxes due to net diffusive transport were considered to be negligible in the pools (see
255 detailed explanation the *interactive discussion*).

256 **Biological activity calculations**

257 The rates of Net Community Calcification (NCC; $\text{mmol CaCO}_3 \text{ m}^{-2} \text{ h}^{-1}$) and Net
258 Community Production (NCP) or Community Respiration (CR; $\text{mmol O}_2 \text{ m}^{-2} \text{ h}^{-1}$ or mmol C m^{-2}
259 h^{-1}) were calculated between two consecutive sampling times. These rates respectively represent
260 the measured changes of net CaCO_3 precipitation and net organic carbon production (or oxygen
261 consumption) by the community. Positive NCC represents net CaCO_3 precipitation (gross
262 precipitation > dissolution) and negative rates represent net dissolution (dissolution >
263 precipitation). NCP is positive when the community primary production exceeds respiration and
264 negative when community primary production is less than respiration. We use CR for nights, when
265 there is no primary production (oxygen consumption and carbon release only).

266 NCC was calculated using the alkalinity anomaly method (Smith and Key, 1975). Briefly,
267 for each mol of CaCO_3 precipitated, two moles of HCO_3^- combine with Ca^{2+} , and TA decreases
268 by two moles (*Eq. 1*). Two independent estimates of NCP (or CR) were calculated, one derived
269 from changes in ΔO_2 (NCP_{O_2} or CR_{O_2}) and one derived from ΔDIC and NCC (NCP_{DIC} or CR_{DIC}).

270 NCC and NCP (or CR) were thus calculated as follows:

$$271 \quad \text{NCC} = \frac{\Delta\text{TA}}{2\Delta t} \times \frac{V}{S} \quad (1)$$

272
$$NCP \text{ (or } CR)_{O_2} = \frac{\Delta O_2}{\Delta t} \times \frac{V}{S} \quad (2)$$

273
$$NCP \text{ (or } CR)_{DIC} = \frac{-\Delta DIC}{\Delta t} \times \frac{V}{S} - NCC \quad (3)$$

274 with ΔTA (mmol L^{-1}), ΔDIC (mmol L^{-1}) and ΔO_2 (mmol L^{-1}) the change in concentration of TA,
 275 DIC and O_2 , between consecutive samples and Δt the duration between consecutive samples (h),
 276 V pool volume (L), S the pool surface area (m^2).

277 Up to seven NCC and NCP (or CR) rates were calculated for each pool during each
 278 emersion period (one per hour). These rates were used to investigate the direct correlation between
 279 biological activity and environmental factors such as light intensity or Ω_a .

280 Rates calculated this way are however not independent from each other (i.e., the rate
 281 measured at $t+2$ is dependent on the rate at $t+1$), limiting further statistical analyses on the effect
 282 of the treatment. This is why, to investigate the effect of pH treatment (“present” vs. “future”) on
 283 community biological activity, we also calculated NCC and NCP or CR using linear regressions
 284 (NCC_{lm} and NCP_{lm} or CR_{lm}) between TA, [DIC] and [O_2] and time after the start of the emersion
 285 period (for detailed results of the regressions, e.g., goodness-of-fit, see **Supp. Mat. LM1-3**). The
 286 few data from diurnal tides that were taken after sunset were excluded from these regressions. For
 287 oxygen, data were limited to the first three hours of emersion as high O_2 concentrations ($>22 \text{ mg}$
 288 L^{-1}) and supersaturation ($>200 \%$) led to inaccurate measurements and/or possible oxygen
 289 degassing afterwards (see **Supp. Mat. LM2**). This regression approach provides a single estimate
 290 of the rate of NCC, NCP_{DIC} (or CR_{DIC}) and NCP_{O_2} (or CR_{O_2}) for each pool during each emersion
 291 period ($n = 17$ diurnal and 6 nocturnal low-tide emersion periods \times 5 pools = 115). These rates
 292 were then used in generalized linear mixed models (GLMM) to assess the effect of pH treatment
 293 on diurnal and nocturnal biological activity (see “*statistical analyses*” below).

294 We calculated community calcification and production budgets (respectively CCB and
 295 CPB) at emersion as an indication of the night/day balance in calcification and production: when
 296 CCB/CPB is positive the pool community calcifies/produces more by day than they
 297 dissolve/respire at night. Both were calculated for winter (February 2020 and 2021) and summer
 298 (September 2020 and 2021) for each pool as follows:

299
$$CCB = NCC_D + NCC_N \quad (4)$$

300
$$CPB = NCP_D + CR_N \quad (5)$$

301 with NCC_D and $NCP_D (> 0)$ the average diurnal NCC and NCP for a given pool for a treatment
302 and a season and NCC_N and $CR_N (< 0)$ the average nocturnal NCC and dark respiration for the
303 same conditions. Three approaches were used for estimating CPB, given the uncertainties of each
304 NCP estimate (see discussion): (1) O_2 -derived estimates of NCP (CPB_{O_2}), (2) DIC- derived
305 estimates (CPB_{DIC}) and (3) a “mixed” approach that combined nocturnal CR_{O_2} and diurnal NCP_{DIC}
306 (CPB_m), under the assumption that one mol of carbon is produced/consumed when one mol of O_2
307 is produced/consumed. Although CPB resemble gross community production in the way the rates
308 are calculated (difference between light and dark net production/respiration rates), if one wanted
309 to reuse these rates for gross community production, they should be do so with care due to
310 differences in night and day temperature (see extended discussion on this subject in Bracken et al.,
311 2022). The treatment effect was assessed on CCB and CPB by comparing the change due to the
312 “future” treatment in each pool.

313

314 **Statistical analyses**

315 All data are presented as mean \pm standard deviation (SD). The analyses were made using the
316 software R (R Core Team, 2017). The level of significance used was 5%. Because data were
317 measured on the same five pools but on different days for different treatments, we used GLMM to
318 test for the effect of treatment on NCC_{lm} and on O_2 and DIC-derived NCP_{lm} (or CR_{lm}), assigning
319 sampling days (i.e., low-tide emersion periods) as the random factor and pools (five levels), mean
320 temperature of the pool during low-tide emersion period (a continuous proxy for season) and
321 treatment (*Treat*: “future” vs. “present”) as fixed factors. This was performed using the R package
322 *nlme* (Pinheiro et al., 2018). Models with and without standardized residuals were compared using
323 ANOVAs and, when different, Akaike Information Criteria (AIC) was used to choose the best
324 fitted-model of the two. For GLMM, mean daily PAR was not used as it has strong collinearity
325 with mean daily temperature/season. We used ANOVAs to test the effect of temperature, pool and
326 treatment on initial (averaged over the first hour of emersion) and final (averaged for > 5 hours
327 after emersion) carbonate chemistry conditions. The normality of the data was tested using
328 Shapiro–Wilk tests and qq-plots, while variance homogeneity was tested with Bartlett tests.

329

330 **RESULTS**

331 **1/ Environmental conditions**

332 **Adjacent waters:** Temperatures (and salinity) measured in the seawater adjacent to the pools were
333 6-7°C in winter (February; salinity S=35.0), 11-12°C in spring (April; S=35.5) and 17-18°C in
334 summer (September; S=36.0). This seawater was characterized by average pH_T of 8.01 ± 0.06
335 units, total alkalinity of $2319 \pm 6 \mu\text{mol kg}^{-1}$, $p\text{CO}_2$ of $445 \pm 69 \mu\text{atm}$, $\Omega_a = 2.2 \pm 0.3$ and $[\text{O}_2] =$
336 $100 \pm 1 \%$ of air saturation (or $10.1 \pm 1.5 \text{ mg L}^{-1}$; n=5).

337 **Light duration and intensity:** In Roscoff, day:night (i.e., no light) periods are typically 10h:14h
338 in February, 14h:10h in April and September. Photosynthetically active radiation (PAR) was two
339 to three times higher in spring/summer (**Fig. 3A:** April/September $\sim 1500 \mu\text{mol m}^{-2} \text{ s}^{-1}$) than in
340 winter (February $\sim 500 \mu\text{mol m}^{-2} \text{ s}^{-1}$).

341 **Carbonate chemistry conditions at the start of the emersion period (< 1h post emersion):**

342 Both for diurnal and nocturnal tides, the initial pH was significantly lower in pools with added
343 CO_2 than in the present-day pools (Day: $pH_T = 8.2 \pm 0.1$ vs. 7.5 ± 0.2 units; Night: 8.0 ± 0.1 vs.
344 7.4 ± 0.1 units for “present” and “future” pools respectively; *Treat* $p < 0.001$; detailed results in
345 **Fig. S2-3, Table S1-2**). This corresponds to $p\text{CO}_2$ of 260 ± 100 vs. $1900 \pm 835 \mu\text{atm}$ (day) and
346 510 ± 90 vs. $2310 \pm 410 \mu\text{atm}$ (night) for pools in “present” and “future” conditions respectively.
347 Adding CO_2 in the pools increased the mean DIC concentration by $320 \mu\text{mol kg}^{-1}$ during the day
348 and $240 \mu\text{mol kg}^{-1}$ during the night. In “present-day” conditions, the pools started at supersaturated
349 levels with regards to aragonite (day: $\Omega_a = 3.3 \pm 1.3$, night: 2.2 ± 0.3). Adding CO_2 significantly
350 decreased Ω_a (*Treat*: $p < 0.001$, **Table S1**) leading to initial “future” conditions often
351 undersaturated with regards to aragonite ($\Omega_a = 0.8 \pm 0.5$) by day and always undersaturated
352 conditions by night ($\Omega_a = 0.6 \pm 0.1$). Furthermore, in “future” diurnal conditions, pools were
353 always undersaturated with respect to aragonite from the start of the emersion period in February
354 ($\Omega_a = 0.5 \pm 0.2$) but not in April ($\Omega_a = 1.1 \pm 0.7$) and September ($\Omega_a = 1.2 \pm 0.5$; **Table S1**). At the
355 start of emersion, total alkalinity was $2303 \pm 34 \mu\text{mol kg}^{-1}$ (similar to adjacent seawater), and
356 uncorrelated with treatment ($p > 0.05$) and temperature ($p > 0.6$).

357 As data was averaged on the first hour post-emersion, the mean initial oxygen
358 concentration calculated was already affected by NCP by day ($14.0 \pm 2 \text{ mg O}_2 \text{ L}^{-1}$) and CR by
359 night ($9.5 \pm 1.5 \text{ mg O}_2 \text{ L}^{-1}$; vs. $10.1 \pm 1.5 \text{ mg O}_2 \text{ L}^{-1}$ for adjacent seawater). This was also visible
360 in CO_2 partial pressure, with lower $p\text{CO}_2$ than expected during the first hour post-emersion by day
361 ($262 \pm 102 \text{ } \mu\text{atm}$ vs. $445 \pm 69 \text{ } \mu\text{atm}$ for adjacent seawater) and higher $p\text{CO}_2$ at night (508 ± 88
362 μatm) in the “present-day” conditions.

363 **2/ Diurnal tides**

364 **Diurnal pool chemistry:** Starting from the aforementioned values at emersion, the pools followed
365 a clear temporal evolution due to solar irradiance and community metabolism (**Fig. 3**). Firstly, we
366 observed increases in salinity (+1.5 units on average, **Fig. 3A**) and temperature (+4°C in
367 September, +6°C in April on average) in summer and spring. In winter, temperatures tended to
368 decrease (-1.7°C on average) with air temperatures colder than that of the seawater; salinity was
369 stable (35.5 ± 0.8).

370 Secondly, we observed positive NCP corroborated by a doubling in oxygen concentration
371 (**Fig. 3A**) a few hours after the start of emersion. In parallel, the seawater DIC concentration
372 decreased by half from the initial concentration (from 2130 ± 195 to $1140 \pm 560 \text{ } \mu\text{mol kg}^{-1}$; **Fig.**
373 **3B**), the range of which largely depended on the season (**Fig. S2**). For instance, in February, DIC
374 consumption in pool seawater averaged $\sim 700 \text{ } \mu\text{mol kg}^{-1}$ over a low-tide period, while it averaged
375 $\sim 1500 \text{ } \mu\text{mol kg}^{-1}$ in September. Particularly extreme conditions, with DIC concentrations
376 effectively reaching $0 \text{ } \mu\text{mol kg}^{-1}$, were observed in two of the pools, at three tides in September
377 2020 (see further details below in “5/ *The particular case of September 2020 tides*”). At the end
378 of diurnal emersions, average $p\text{CO}_2$ was always below $100 \text{ } \mu\text{atm}$, reaching as low as $1 \pm 2 \text{ } \mu\text{atm}$
379 in September (**Fig. 3B, Table S1**). As a result, diurnal pH_T increased to 9.1 ± 0.6 by the end of
380 emersion, with maximum values up to 10.3 in summer (**Fig. 3B**). At the end of a diurnal emersion
381 period, the pools’ pH was stable, reaching either a plateau or decreasing after sunset (see PAR in
382 **Fig. 3A**). Similarly, at the end of diurnal emersion periods, Ω_a was high (5.6 ± 3.0 on average;
383 max 10.4). Lastly, we observed a diurnal decrease in TA by $415 \text{ } \mu\text{mol kg}^{-1}$ on average, indicative
384 of net calcification.

385 It is noteworthy that the carbonate chemistry conditions experienced at the end of diurnal
386 emersion converged whatever the initial treatment (**Fig. S2, Table S1**). For instance, while Ω_a was
387 significantly different between treatments at the start of the emersion period, both treatments
388 reached similar Ω_a at the end of emersion (> 5 h) of around 5.3 ± 2.2 (ANOVA: Treat: $p = 0.1$,
389 Temp: $p = 0.002$, Pool: $p = 0.01$). There was less convergence for pH_T where, even five hours after
390 emersion, there were still statistically significant, albeit small, differences between treatments (p
391 < 0.001 for pH_T with 9.2 ± 0.6 for “present” and 9.0 ± 0.6 for “future” pools).

392 **Diurnal biological activity:** Net community production was positive during daytime, except at
393 sunset (**Fig. 3C**). NCP was significantly correlated to light intensity (PAR) and further results for
394 hourly NCP and their correlation to hourly averaged PAR, Ω_a and temperature can be found in the
395 **Supp. Mat. (Fig. S6 and S7)**.

396 As expected, seasons/temperature affected net oxygen production (O_2 -derived NCP_{lm}),
397 increasing from 7 ± 3 $\text{mmol O}_2 \text{ m}^{-2} \text{ hr}^{-1}$ in February to 18 ± 11 $\text{mmol O}_2 \text{ m}^{-2} \text{ hr}^{-1}$ in September
398 (**Fig. 4A and Table 2A**: GLMM, $p < 0.001$). CO_2 addition increased O_2 -derived NCP_{lm} by 20%
399 on average over all seasons, from 10 ± 7 $\text{mmol O}_2 \text{ m}^{-2} \text{ hr}^{-1}$ in “present” conditions to 12 ± 9 mmol
400 $\text{O}_2 \text{ m}^{-2} \text{ hr}^{-1}$ ($p = 0.0015$). Net oxygen production differed across pools ($p < 0.003$), with
401 significantly more productivity in pool C (17.6 ± 12.7 $\text{mmol O}_2 \text{ m}^{-2} \text{ hr}^{-1}$) and D (10.6 ± 5.6 mmol
402 $\text{O}_2 \text{ m}^{-2} \text{ hr}^{-1}$), compared to the pools A, B and E (8.1 ± 4.1 $\text{mmol O}_2 \text{ m}^{-2} \text{ hr}^{-1}$).

403 Results are similar for DIC-derived NCP_{lm} (**Fig. 4A and Table 2B**), with primary
404 production ranging from 6 ± 2 $\text{mmol C m}^{-2} \text{ hr}^{-1}$ in February up to 12 ± 5 $\text{mmol C m}^{-2} \text{ hr}^{-1}$ in
405 September ($p < 0.001$). As for O_2 -derived NCP_{lm} CO_2 addition increased DIC-derived NCP_{lm} by
406 20 % on average over all seasons ($p < 0.001$, **Fig. 4A**). This increase was particularly apparent in
407 the summer, where NCP_{lm} increased from 11 ± 4 $\text{mmol m}^{-2} \text{ hr}^{-1}$ in the “present” treatment to $15 \pm$
408 5 $\text{mmol C m}^{-2} \text{ hr}^{-1}$ in the “future” treatment (+ 35 %). Productivity (NCP_{lm}) was significantly lower
409 in pools B and E than in pool A, and significantly higher in pools C and D ($p < 0.003$).

410 By day, with the exception of sunset, net community calcification was positive (NCC and
411 $\text{NCC}_{\text{lm}} > 0$: **Fig. 3C and 4B**) and occurred in an environment that was supersaturated with regards
412 to aragonite (**Fig. 3B**). This was with the exception of a few emersion periods in September 2020
413 where dissolution was observed despite high saturation state conditions (further details below).

414 Similar to NCP_{lm} , diurnal net calcification rates (NCC_{lm}) were strongly influenced by
 415 temperature/season (**Fig. 4B** and **Table 2C**: GLMM, $p < 0.001$) ranging from 1.2 ± 0.5 mmol
 416 $CaCO_3$ m^{-2} hr^{-1} in February to 3.3 ± 1.3 mmol $CaCO_3$ m^{-2} hr^{-1} in September. NCC hourly rates
 417 positively correlated with averaged Ω_a ($p < 0.0001$; $NCC = 0.15 \times \Omega_a + 0.85$; linear regression
 418 presented in **Fig. S7**), significantly but not strongly ($R^2 = 10\%$). CO_2 addition did not influence
 419 NCC_{lm} rates during the day ($p = 0.47$). However, NCC_{lm} did differ across pools ($p < 0.003$): rates
 420 were relatively low in pool E – lowest CCA cover (30%) – (1.4 ± 1.4 mmol $CaCO_3$ m^{-2} hr^{-1}), and
 421 high in pool D – highest CCA cover (70%) – (2.2 ± 0.8 mmol $CaCO_3$ m^{-2} hr^{-1}) compared to the
 422 three other pools (2.0 ± 1.25 mmol $CaCO_3$ m^{-2} hr^{-1}).

423 **Table 2: Results of the generalized linear mixed-effect models for A) O_2 -derived NCP_{lm}**
 424 **(mmol O_2 m^{-2} hr^{-1}), B) DIC-derived NCP_{lm} (mmol C m^{-2} hr^{-1}) and C) NCC_{lm} (mmol $CaCO_3$ m^{-2}**
 425 **hr^{-1}) during the day and night.** The models include three fixed factors: *Temp* (mean temperature:
 426 a continuous factor), *Treat* (for CO_2 “future” treatment vs. “present”, two levels) and *pools* (vs. A,
 427 five levels), and one random effect (*low-tide emersion period* or the calendar day at which the pool
 428 was measured). Significant p -values are highlighted in bold.

429

A.	O_2 -derived NCP_{lm}		Estimate	Standard Error	p -value
Day	Intercept		1.49	1.37	0.28
	Fixed Effects	<i>Temp</i>	0.54	0.13	<0.001*
		<i>Treat</i>	1.09	0.33	0.0015*
		<i>Pools</i>	A, B, E \neq C, D		
	Random Effect	<i>Low-tide emersion period</i>	8.90	0.90	<0.001*
Night	Intercept		2.87	0.98	0.005*
	Fixed Effects	<i>Temp</i>	-0.43	0.06	<0.001*
		<i>Treat</i>	-0.25	0.28	0.39
		<i>Pools</i>	A, B, D \neq C, E		
	Random Effect	<i>Low-tide emersion period</i>	-3.46	0.87	<0.001*

430

B.	DIC-derived NCP_{1m}	Estimate	Standard Error	p-value	
Day	Intercept	2.3	1.08	0.035*	
	Fixed Effects	<i>Temp</i>	0.38	0.08	<0.001*
		<i>Treat</i>	1.25	0.25	<0.001*
		<i>Pools</i>	A ≠ B, C, D, E		<0.003*
	Random Effect	<i>Low-tide emersion period</i>	7.7	0.7	<0.001*
Night	Intercept	-0.94	1.4	0.51	
	Fixed Effects	<i>Temp</i>	-0.92	0.19	0.053
		<i>Treat</i>	-0.25	0.28	<0.001*
		<i>Pools</i>	A, B, D, E ≠ C		0.016*
	Random Effect	<i>Low-tide emersion period</i>	1.61	0.57	0.01*

C.	NCC _{lm}		Estimate	Standard Error	p-value
Day	Intercept		-0.16	0.31	0.61
	Fixed Effects	<i>Temp</i>	-0.13	0.02	< 0.001 *
		<i>Treat</i>	0.06	0.08	0.47
		<i>Pools</i>	A, B, C ≠ D, E		< 0.003 *
	Random Effect	<i>Low-tide emersion period</i>	-1.90	0.24	< 0.001 *
Night	Intercept		0.64	0.26	0.026 *
	Fixed Effects	<i>Temp</i>	0.009	0.016	0.57
		<i>Treat</i>	0.28	0.07	0.0017 *
		<i>Pools</i>	A, B, C ≠ D, E		< 0.017 *
	Random Effect	<i>Low-tide emersion period</i>	0.83	0.078	< 0.001 *

433

434 3/ Nocturnal tides

435 **Nocturnal pool chemistry:** Seawater temperatures during the nights were stable (**Fig. 3A**)
436 throughout the emersion period in summer (from $17.3 \pm 0.4^\circ\text{C}$ < 1 h post-emersion to $17.2 \pm 0.2^\circ\text{C}$
437 > 5 h post-emersion) and winter (from $8.4 \pm 1.4^\circ\text{C}$ to $7.8 \pm 2.7^\circ\text{C}$ in February; no April nights).
438 We highlight the wide range of winter seawater temperatures with an exceptionally cold tidal cycle
439 (5°C on the 13th of February 2021) due to air temperatures of $3\text{-}4^\circ\text{C}$ (observations from the Île de
440 Batz meteorological station). There was a decline in salinity at night in some winter emersion
441 periods (**Fig. 3A**), due to high air humidity and/or rain. Data where salinity dropped by more than
442 1.5 units in less than an hour were removed from further analyses on net community calcification
443 and respiration.

444 After five hours of emersion, O_2 concentration had decreased by half (from $10.1 \pm 1.5 \text{ mg}$
445 $\text{O}_2 \text{ L}^{-1}$ to $4.9 \pm 3.3 \text{ mg O}_2 \text{ L}^{-1}$) (**Fig. 3A**) due to community respiration. Simultaneously, pH_T
446 decreased to 7.6 ± 0.2 (“present”) or stayed at 7.4 ± 0.2 (“future”; **Fig. 3B and S2, Table S1**), with
447 significant effects of pools, treatment and temperature ($p < 0.001$ for all three). DIC concentration
448 increased by $+256 \mu\text{mol kg}^{-1}$ on average over an emersion period. The range of this increase
449 depended on the temperature and the pool: in winter ($5\text{-}10^\circ\text{C}$), present-day pool seawater gained
450 $+130 \mu\text{mol kg}^{-1}$ ($+60$ for “future” pools) of DIC over an emersion period, when in summer they
451 gained $+370 \mu\text{mol kg}^{-1}$ for “present” (“future”: $+310 \mu\text{mol kg}^{-1}$) pools (**Fig. S3**). Saturation state
452 converged towards similar undersaturated levels at night (**Fig. 3B and S2, Table S1**): Ω_a stayed
453 stable in the “future” treatment (0.7 ± 0.2 units on average) and decreased in the “present-day”
454 treatment (-1.2 units from initial Ω_a). At the end of nocturnal emersion Ω_a were still statistically
455 different due to the initial treatment ($p < 0.001$ for *Treat*, *Temp* and *Pools*).

456 **Nocturnal biological activity:** At night, oxygen was consumed, i.e., we observed dark respiration
457 (CR; **Fig. 3C**). Community respiration (O_2 -derived CR_lm) varied according to season (**Fig. 4A** and
458 **Table 2A**: $p < 0.001$): temperature linearly increased nocturnal respiration rates from -1.0 ± 1.2
459 $\text{mmol O}_2 \text{ m}^{-2} \text{ hr}^{-1}$ in February to $-4.7 \pm 1.3 \text{ mmol O}_2 \text{ m}^{-2} \text{ hr}^{-1}$ in September. The CO_2 treatment did
460 not influence night respiration ($p = 0.39$). Respiration rates were significantly influenced by pools
461 ($p = 0.03$), probably linked to the relative biomass of heterotrophs and autotrophs; respiration was
462 significantly higher in pool C ($-4.6 \pm 2.8 \text{ mmol O}_2 \text{ m}^{-2} \text{ hr}^{-1}$) and significantly lower in pool E (-2.4
463 $\pm 1.4 \text{ mmol O}_2 \text{ m}^{-2} \text{ hr}^{-1}$) than in pools A, B and D ($-3.4 \pm 2.1 \text{ mmol O}_2 \text{ m}^{-2} \text{ hr}^{-1}$).

464 Night respiration estimated using DIC and NCC was near zero ($CR_{lm} = -0.2 \pm 0.7 \text{ mmol m}^{-2}$
465 hr^{-1}). At these low rates, uncertainties associated with much higher rates of net dissolution
466 (negative NCC) sometimes led to spuriously positive DIC-derived CR estimates, hindering
467 interpretation. Nevertheless, DIC-derived community respiration was ten times lower in February
468 than in September (-0.2 ± 0.7 and $-2.3 \pm 1.1 \text{ mmol C m}^{-2} \text{ hr}^{-1}$ respectively), although it was not
469 linearly driven by temperature ($p = 0.053$; **Fig. 4B** and **Table 2B**). Adding CO_2 to the pools
470 influenced DIC-derived community respiration in a way that was inverse to that seen with O_2 , but
471 as stated above, this was likely an artifact of subtracting NCC from small DIC changes. As for O_2 ,
472 DIC-derived CR_{lm} significantly changed depending on the pools.

473 At night, the pools experienced significant net community dissolution ($NCC < 0$; **Fig. 3C**)
474 even when waters were supersaturated with regards to aragonite in the “present” treatment (**Fig.**
475 **3B**: $\Omega_a > 1$). Nocturnal net dissolution rates (NCC_{lm}) were not significantly affected by temperature
476 in the range investigated ($5\text{-}18^\circ\text{C}$; **Fig. 4C** and **Table 2C**; $p = 0.57$). However, adding CO_2 in the
477 pools increased net dissolution rates ($p = 0.0017$) from $-0.7 \pm 0.3 \text{ mmol CaCO}_3 \text{ m}^{-2} \text{ hr}^{-1}$ to $-1.0 \pm$
478 $0.4 \text{ mmol CaCO}_3 \text{ m}^{-2} \text{ hr}^{-1}$ (+40 %). Similarly, looking instead at hourly rates (NCC), dissolution
479 correlated significantly ($p < 0.0001$) with Ω_a ($NCC = 0.34 \times \Omega_a - 1.22$; $R^2 = 11 \%$; **Fig. S7**). The
480 strength of this correlation depended on seasons and pools (**Fig. S8**). Net dissolution rates (NCC_{lm})
481 significantly differed by pool ($p < 0.0017$): the lowest rates were observed in pool E (-0.4 ± 0.2
482 $\text{mmol CaCO}_3 \text{ m}^{-2} \text{ hr}^{-1}$) – the pool with the lowest CCA cover –, and the highest dissolution in pool
483 D – the pool with the highest CCA cover (-1.0 ± 0.4 vs. $-0.9 \pm 0.3 \text{ mmol CaCO}_3 \text{ m}^{-2} \text{ hr}^{-1}$ for A, B
484 and C).

485

486 **4/ Influence of the treatment on CPB and CCB**

487 Pools fixed more carbon during the day than they respired at night, i.e., the community production
488 budget (CPB: balance between night and day) was positive in all the pools, both in winter and
489 summer and whatever the treatment (**Fig. 5**). CPB_{DIC} and CPB_m estimates were typically lower
490 than CPB_{O_2} (in 14/20 cases and 18/20 cases respectively). The production budget was significantly
491 lower in winter than in summer (FEB: $CPB_{O_2} = 3 \pm 1 \text{ mmol O}_2 \text{ m}^{-2} \text{ h}^{-1}$, SEP: $7 \pm 5 \text{ mmol O}_2 \text{ m}^{-2}$
492 h^{-1} ; t-test: $t = -2.4$, $df = 9.8$, $p = 0.03$). Adding CO_2 increased CPB in all the pools in summer by +
493 $3.0 \pm 2.1 \text{ mmol O}_2 \text{ m}^{-2} \text{ h}^{-1}$, an increase in production by 50 to 80 % (ΔCPB ; **Fig. 5**). In winter, there

494 was no evidence of such a “fertilization effect” across the most accurate CPB estimates for this
495 season (CPB_{O_2} , CPB_m): we only observed a significant increase in production due to CO_2 addition
496 in two of the pools (+60 % to +120 % for A and B). For the three other pools, CPB either induced
497 minimal changes (< 20 % for C and E) or a decrease in production (D: down to -34 %). DIC-
498 derived ΔCPB in winter (all positive) should be interpreted with caution since some nocturnal
499 CR_m were spuriously positive in the “future” treatment (see “*nocturnal biological activity*” above).

500 The pools calcified more during the day than they dissolved at night ($CCB > 0$), both in
501 summer and winter (**Fig. 5**). CCB was significantly lower in winter than in summer (FEB: $CCB =$
502 0.2 ± 0.2 mmol $CaCO_3$ $m^{-2} h^{-1}$, SEP: 1.2 ± 0.6 mmol $CaCO_3$ $m^{-2} h^{-1}$; t-test: $t = -5.2$, $df = 11.7$, $p =$
503 0.0002). In winter, adding CO_2 decreased CCB by more than 80 % in pools C, D, and E (**Fig. 5**).
504 The CO_2 addition even resulted in a transition from a positive community calcification balance to
505 dissolution in pool C (133 % change, from +0.5 to -0.2 mmol $CaCO_3$ $m^{-2} h^{-1}$). For the two other
506 pools (A and B), winter CO_2 addition increased their relatively small calcification balance (A: +87
507 %, from 0.1 to 0.2 mmol $CaCO_3$ $m^{-2} h^{-1}$ and B: +71 %, from 0.2 to 0.3 mmol $CaCO_3$ $m^{-2} h^{-1}$). In
508 summer, changes in CCB due to treatment appeared minimal in pools A, B and E (< 15 % change)
509 and either increased (C: +67%) or decreased (D: -57%) in the two other pools.

510

511 **5/ The particular case of September 2020 tides**

512 During diurnal tides of September 2020 (high PAR and high temperature summer conditions), we
513 observed an unexpected phenomenon: dissolution occurred at extremely high pH_T values (9-10)
514 in pools C and E (**Fig. 6**). Under these conditions effectively all the seawater DIC in these pools
515 was consumed by photosynthesis and calcification ($DIC \approx 0$ mmol kg^{-1}) four hours after emersion.
516 As such, the CO_3^{2-} concentration was also effectively zero and the pools reached very low
517 saturations states ($\Omega_a \approx 0$) despite high pH (**Fig. 6**). These conditions were quickly followed by
518 indicators of $CaCO_3$ dissolution (increasing TA and DIC) instead of the expected diurnal
519 precipitation. It is therefore noteworthy that dissolution may happen at high pH, and that pH and
520 Ω can decorrelate (**Fig. 7**) in situations with high photosynthesis and limited mixing of water
521 masses.

522

523 **DISCUSSION**

524 Temperate tidal pools are environments of extreme variability. In our pools, we observed seawater
525 temperatures that could increase by up to 10°C in a few hours compared to the adjacent ocean.
526 During diurnal emersion periods, oxygen concentrations doubled and pH could increase to pH 10
527 in present-day summer conditions. At night, pH routinely reached levels usually used as the
528 “treatment” for ocean acidification perturbation experiments (~7.6). Organisms present in the tidal
529 pools may therefore already be adapted or acclimatized to extreme variability in pH and saturation
530 state, which could affect their responses to ocean acidification (Andersson et al., 2015). For
531 example, CCA from a site with naturally high $p\text{CO}_2$ variability calcified ~50 % more than
532 individuals from a nearby site of low variability when submitted to oscillating high $p\text{CO}_2$
533 treatments (Johnson et al., 2014). Here we show that, even in intertidal communities likely already
534 acclimated or adapted to variable conditions, with potentially large phenotypic plasticity,
535 acidification can still modify net community production and calcification rates.

536 **Diurnal fertilization under CO₂ addition**

537 Adding CO₂ to simulate future seawater acidification in the pools led to a diurnal fertilization
538 effect. The community’s net primary production increased by 20% on average across all seasons,
539 which was particularly visible in summer (+ 35%), when temperatures/metabolic rates were high.
540 Adding CO₂, we also added substrate for photosynthesis in the form of DIC (**Fig. 3B**) that the
541 algae of the pools can assimilate, potentially supporting higher DIC use and algal primary
542 production. This effect was apparent from the start of the emersion, suggesting a direct effect of
543 increasing DIC concentration in the pools. It seems that photosynthesis in the pools was carbon-
544 limited and that carbon addition therefore enhanced primary production, in winter and to an even
545 greater extent in summer. During photosynthesis, the uptake of inorganic carbon leads to a
546 significant decrease in DIC - even in present-day conditions. Intertidal algae are typically adapted
547 to this with coralline algae in particular containing CCMs (CO₂ concentrating mechanisms) that
548 allow them to achieve primary production in low DIC concentrations (Raven, 2011). Increasing
549 seawater DIC may however promote an increase in active and/or passive CO₂ and HCO₃⁻ fluxes
550 towards photosynthetic compartments. Borowitzka (1981) found that the photosynthetic rate of an
551 intertidal CCA was highest at pH 6.5 to 7.5 (increased from pH 8.1), a change in pH that was
552 achieved using HCl, suggesting that increased photosynthetic activity could also be linked to

553 proton gradients/pumps and/or decreased energy expenditure needed to operate CCMs rather than
554 directly related to CO₂ gradients or higher substrate availability.

555 In winter and summer, pools in present-day and future conditions were autotrophic at
556 emersion ($NCP_D > CR_N$, **Fig. 5**). If we consider the CPB as integrated diurnal NCP and nocturnal
557 CR over 24 hours (assuming equal day:night duration), this means that the pools always fixed
558 more carbon during the day than they respired at night at emersion ($NCP \gg CR$), regardless of
559 treatment. One methodological uncertainty we highlight regarding net production is that diurnal
560 DIC-derived NCP estimations were 50 % higher than O₂-derived NCP estimates (**Fig. 3C and Fig.**
561 **4**, $NCP_{DIC} = 1.6 \pm 0.05 NCP_{O_2}$ by day; $R^2 = 75 \%$). This discrepancy was far less apparent during
562 nights, when methods agreed on respiration rates ($CR_{DIC} = 1.0 \pm 0.09 CR_{O_2}$; $R^2 = 56 \%$). While
563 O₂-derived NCP appears accurate during the night, O₂ production during the day is likely to have
564 been underestimated due to degassing (e.g., visible formation of oxygen bubbles at the surface of
565 algae, >150 % air saturation by day vs. < 100 % at night). Thus, estimating diurnal net production
566 using oxygen measurements may not be appropriate in algae-dominated environments such as
567 these tidal pools. Nevertheless, despite the difference in absolute NCP estimates, both approaches
568 indicate a diurnal fertilization effect.

569

570 **Nocturnal dissolution under CO₂ addition**

571 In the present study, natural mesocosms - temperate coralline-dominated tidal pools - were used
572 to investigate the effect of ocean acidification on net calcification at the community level. As we
573 observed a fertilization effect of CO₂ addition by day, we could have expected that it would also
574 enhance diurnal calcification – as photosynthesis and calcification are tightly linked (Martin et al.,
575 2013; Martin et al., 2013; Williamson et al., 2017) -, but this was not observed. Treatment had no
576 significant effect on the daytime net calcification rates, and diurnal variability in calcification
577 appears to be predominately driven by PAR, temperature, and metabolic activity (NCP). Increasing
578 metabolic rates - in turn increasing calcification rates - may have however counterbalanced any
579 calcification suppression or increased dissolution due to acidification, making its effect invisible.
580 Noisette et al. (2013) similarly found no effect of *p*CO₂ treatment on light calcification for *E.*
581 *elongata*. However, the authors reported a significant decrease in light calcification in *L.*
582 *incrustans*, net calcification even switched to net dissolution in 750 and 1000 μ atm *p*CO₂
583 treatments. While our “future” treatments started at *p*CO₂ levels higher than 1000 μ atm, the fact

584 that CO₂ addition did not influence diurnal calcification could also be due to favorable saturation
585 state conditions in the micro-environment in which calcification occurs. The diffusive boundary
586 layer (DBL) can enhance CaCO₃ precipitation micro-environment conditions due to the uptake of
587 CO₂/DIC for photosynthesis. For instance, in light conditions, CCA surface pH has been shown to
588 reach as high as 8.6 (Houlihan et al., 2020) in surrounding seawater at pH 7.7 (+1.1 pH units),
589 which would be highly favorable to calcification. Although there are conflicting results indicating
590 that saturation state of the ambient seawater is a key driver of coralline algal calcification, the
591 biomineralization process in coralline algae has also been shown to present a certain degree of
592 biological control (de Carvalho et al., 2017; Nash et al., 2019). Recent work using boron isotopes
593 ($\delta^{11}\text{B}$) as a proxy for pH showed that coralline algae have ability to elevate pH at their site of
594 calcification (Cornwall et al., 2017). But more complex interactions may also be at work, e.g.,
595 CCA may use increases in HCO₃⁻ (due to CO₂ dissolution) to calcify, making them more resistant
596 to ocean acidification, as suggested by Comeau et al. (2013).

597 There was net CaCO₃ dissolution in the pools at night (-0.7 mmol CaCO₃ m⁻² hr⁻¹), even
598 when waters were still supersaturated with regards to aragonite under present-day conditions.
599 Night dissolution may be a sign that the DBL of the calcifiers inhabiting the pools is
600 undersaturated, possibly as a result of respiration. Indeed, Houlihan et al. (2020) observed that
601 nocturnal algal respiration by CCA, increased CO₂ in the DBL, decreasing pH of the DBL by 0.1
602 units. Such a small pH decrease is unlikely to explain alone an undersaturation of the calcifying
603 environment as aragonite saturation state was still above 1.2 in most of the “present-day”
604 conditions. However, given the solubility of high-Mg calcite - the mineral composing *L. incrustans*
605 and *E. elongata* in particular (Ries, 2011) - can be twice that of aragonite (Sulpis et al., 2021;
606 Yamamoto et al., 2012), it is possible that undersaturation already occurs at night for this mineral
607 even for $\Omega_a > 1$. Another reason for night dissolution might be linked to the patellid limpet, an
608 opportunistic (Schaal and Grall, 2015) and dominant grazer in rockpools, that can be particularly
609 active at night (Lorenzen, 2007). Encrusting coralline algae can be an important food source for
610 these herbivores and the large percentage of grazed coralline algal CaCO₃ in their gut (Maneveldt
611 et al., 2006) could dissolve easily at night.

612 Adding CO₂ (from 445 to 1500-2000 μatm) at the start of emersion significantly increased
613 net dissolution (NCC_{lm}), by 40 % in summer and 70 % in winter. In a previous single-species
614 experiment, Noisette et al. (2013) demonstrated that - for *L. incrustans* from an area close to our

615 site – dark dissolution doubled with increasing $p\text{CO}_2$ (1000 μatm vs. 380 μatm), unlike *E. elongata*,
616 for which there was no effect of $p\text{CO}_2$: the ACA even calcified in the dark up to 750 μatm (see
617 also similar results from Egilsdottir et al., 2013). Since *L. incrustans* is the major calcifying species
618 of the tidal pools we studied, it is likely this species drives the results we observed at the pool
619 community scale. Regardless of the treatment, nocturnal net dissolution rates (NCC) were also
620 significantly correlated with Ω_a , results similar to those found by Kwiatkowski et al. (2016) in
621 temperate tidal pools of California, without CO_2 addition.

622 In summer, pools in present-day and future conditions were precipitative ($\text{CCB} > 0$),
623 meaning that diurnal net calcification exceeded nocturnal net dissolution, regardless of treatment.
624 Adding CO_2 in summer did not consistently change CCB, with most pools showing little change
625 in CCB due to treatment. By contrast, in the colder winter, the calcification budget was at least 50
626 % lower than in summer (“present”), with some pools that had comparable net calcification during
627 the day to net dissolution at night. During this season, adding CO_2 had variable impacts on CCB,
628 decreasing it in three of the pools by more than 80 % and increasing relatively small CCB in two.
629 These variable effects may be due to differences in community composition and highlight the
630 difficulty in generalizing the results of natural mesocosm manipulations in which the initial
631 community composition is not controlled. Nevertheless, we expected CO_2 addition to have a
632 greater negative effect in winter (more dissolution) than in summer, with saturation states being
633 lower due to colder temperatures, making it more of a “crucial”/ “bottleneck” season. This
634 emphasizes the need to study the effect of ocean acidification across seasons and temperature
635 ranges, especially given the associated changes in algal community composition and metabolic
636 activity.

637 A limit of the CCB in the current study is that we only considered the tidal pools as closed (emersed)
638 systems. However, in an acidifying ocean, tidal pool communities are submersed for nearly 12 hours per
639 day, resulting in long exposure to low pH. More accurate and realistic budgets would need to integrate these
640 immersion periods, which might have additive negative effects on calcification (see e.g., Legrand et al.,
641 2018b for tidal assemblage experiments on net production/respiration).

642

643 **Instances of aragonite undersaturation at high pH**

644 An unexpected phenomenon happened in the pools C and E in summer: although we measured
645 very high pH values, we observed that total alkalinity suddenly increased, a sign of fast net
646 dissolution. When we then computed the carbonate chemistry, the saturation states were

647 surprisingly low ($\Omega_a = 0$ for $\text{pH}_T = 10$), which was due to near-zero DIC concentrations – and thus
648 near-zero CO_3^{2-} concentrations. In these particular conditions, which occurred towards the end of
649 the tidal emersion period, any CaCO_3 precipitation was less than dissolution; precipitation may
650 even have been impossible due to a lack of DIC substrate. In intertidal pools with a high density
651 of *Zostera marina*, Miller & Kelley (2021) observed a similar decoupling between pH and Ω_a with
652 increases in pH not leading to an increase in saturation state at high pH values due to a lack of
653 DIC/ CO_3^{2-} . In our study, we observed even more drastic decoupling between expected changes in
654 pH, Ω_a and NCC, with some of the fastest net dissolution rates observed at very high pH and very
655 low Ω_a values that were a consequence of near complete consumption of DIC by community
656 production (**Fig. 7**). Macroalgae cultivation has been proposed as a method of bioremediation to
657 local acidification, in particular to improve aquaculture environments (e.g., Bergstrom et al., 2019;
658 Gao & Beardall, 2022): increase in algal or marine plant cover would reverse or buffer the negative
659 effects of acidification on heterotroph calcifiers. Our results and those of Miller & Kelley (2021)
660 suggest that phytoremediation should not consider pH as the sole indicator for “acidification
661 remediation”, and that periodical decreases in saturation state in macroalgae- or seaweed-
662 dominated environments in summer (and during marine heatwaves), may need to be considered
663 for these proposed types of remediations.

664

665 **Conclusion**

666 Relative to its area, human societies are disproportionately reliant on the coastal ocean for the
667 provision of natural resources and climate regulation. Yet our understanding of how anthropogenic
668 carbon emissions and associated ocean acidification will influence natural coastal ecosystems and
669 community metabolism remains limited. In the present study, we manipulated the carbonate
670 chemistry of natural temperate intertidal pools to explore the potential impact of future ocean
671 acidification on community-level calcification and production. We find evidence of large seasonal,
672 diel and community-specific differences in the sensitivity of intertidal community metabolism to
673 acidification. Diurnally, acidification was found to enhance net community production, with this
674 “fertilization effect” indicating algal photosynthesis is naturally carbon limited in such
675 environments at emersion. Diurnal net community calcification was unaffected by acidification.
676 In contrast, nocturnal acidification resulted in greater net community dissolution in the intertidal
677 pools yet had no consistent effect on community respiration. Integrated over day/night emersion

678 periods, the intertidal mesocosms maintained positive net community calcification and production
679 under both present-day and future conditions. Albeit considerable differences between individual
680 pools and strong seasonal dependencies, our results indicate that the net calcification and
681 production of temperate intertidal communities - likely acclimated/adapted to variable conditions
682 - could be affected by future acidification.

683

684 **ACKNOWLEDGEMENTS**

685 We thank Elsa Perruchini, Léonard Dupont, Corentin Clerc, Priscilla Le Mezo, Alban Planchat,
686 Maud Chevalier, Anne Cornillon, Annabel Antheaume, Mailys Roux and Clarisse Dufaux for their
687 kind assistance with fieldwork. This project is fully funded by the CHANEL research chair:
688 *Understanding the Linkages between the Ocean, the Carbon Cycle, and Marine Ecosystems under*
689 *Climate Change*. Data presented for adjacent Atlantic waters characteristics (main text and the
690 supplementary material) were kindly provided by the SOMLIT network database (Service
691 d'Observation en Milieu Littoral; www.somlit.fr) on June 2022.

692

693 **AUTHORS CONTRIBUTIONS**

694 ND, SM and LK designed the experiments and ND carried them out with help from all co-authors.
695 ND analysed the data and prepared the manuscript, with contributions from all co-authors.

696

697 **COMPETING INTERESTS**

698 The authors declare that they have no conflict of interest.

699

700 **DATA AVAILABILITY**

701 Raw data and linear regression model results are provided as supplementary in the Appendix.

702

703 **BIBLIOGRAPHY:**

- 704 Albright, R., Caldeira, L., Hosfelt, J., Kwiatkowski, L., Maclaren, J. K., Mason, B. M., Nebuchina, Y.,
705 Ninokawa, A., Pongratz, J., Ricke, K. L., Rivlin, T., Schneider, K., Sesboüé, M., Shamberger, K., Silverman,
706 J., Wolfe, K., Zhu, K., and Caldeira, K.: Reversal of ocean acidification enhances net coral reef
707 calcification, *Nature*, 531, 362–365, <https://doi.org/10.1038/nature17155>, 2016.
- 708 Albright, R., Takeshita, Y., Koweek, D. A., Ninokawa, A., Wolfe, K., Rivlin, T., Nebuchina, Y., Young, J., and
709 Caldeira, K.: Carbon dioxide addition to coral reef waters suppresses net community calcification,
710 *Nature*, 555, 516–519, <https://doi.org/10.1038/nature25968>, 2018.
- 711 Aminot, A. and Kérouel, R.: Dosage automatique des nutriments dans les eaux marines: méthodes en
712 flux continu, Editions Quae, 191 pp., 2007.
- 713 Andersson, A. J., Kline, D. I., Edmunds, P. J., Archer, S. D., Bednaršek, N., Carpenter, R. C., Chadsey, M.,
714 Goldstein, P., Grottoli, A. G., Hurst, T. P., King, A. L., Kübler, J. E., Kuffner, I. B., Mackey, K. R. M., Menge,
715 B. A., Paytan, A., Riebesell, U., Schnetzer, A., Warner, M. E., and Zimmerman, R. C.: Understanding ocean
716 acidification impacts on organismal to ecological scales, *Oceanography*, 28, 16–27, 2015.
- 717 Barry, J., Hall-Spencer, J., and Tyrrell, T.: In situ perturbation experiments: natural venting sites,
718 spatial/temporal gradients in ocean pH, manipulative in situ $p\text{CO}_2$ perturbations, in: Guide to best
719 practices in ocean acidification research and data reporting, Luxembourg, 123–136, 2010.
- 720 Bergstrom, E., Silva, J., Martins, C., and Horta, P.: Seagrass can mitigate negative ocean acidification
721 effects on calcifying algae, *Sci. Rep.*, 9, 1932, <https://doi.org/10.1038/s41598-018-35670-3>, 2019.
- 722 Borowitzka, M. A.: Photosynthesis and calcification in the articulated coralline red algae *Amphiroa*
723 *anceps* and *A. foliacea*, *Mar. Biol.*, 62, 17–23, <https://doi.org/10.1007/BF00396947>, 1981.
- 724 Bracken, M. E. S., Miller, L. P., Mastroni, S. E., Lira, S. M., and Sorte, C. J. B.: Accounting for variation in
725 temperature and oxygen availability when quantifying marine ecosystem metabolism, *Sci. Rep.*, 12:825,
726 <https://doi.org/10.1038/s41598-021-04685-8>, 2022.
- 727 de Carvalho, R. T., Salgado, L. T., Amado Filho, G. M., Leal, R. N., Werckmann, J., Rossi, A. L., Campos, A.
728 P. C., Karez, C. S., and Farina, M.: Biomineralization of calcium carbonate in the cell wall of
729 *Lithothamnion crispatum* (Hapalidiales, Rhodophyta): correlation between the organic matrix and the
730 mineral phase, *J. Phycol.*, 53, 642–651, <https://doi.org/10.1111/jpy.12526>, 2017.
- 731 Cocquempot, L., Delacourt, C., Paillet, J., Riou, P., Aucan, J., Castelle, B., Charria, G., Claudet, J., Conan,
732 P., Coppola, L., Hocdé, R., Planes, S., Raimbault, P., Savoye, N., Testut, L., and Vuillemin, R.: Coastal
733 ocean and nearshore observation: a French case study, *Front. Mar. Sci.*, 6, 2019.
- 734 Comeau, S., Carpenter, R. C., and Edmunds, P. J.: Coral reef calcifiers buffer their response to ocean
735 acidification using both bicarbonate and carbonate, *Proc. R. Soc. B Biol. Sci.*, 280, 20122374,
736 <https://doi.org/10.1098/rspb.2012.2374>, 2013.
- 737 Cornwall, C. E., Comeau, S., and McCulloch, M. T.: Coralline algae elevate pH at the site of calcification
738 under ocean acidification, *Glob. Change Biol.*, 23, 4245–4256, <https://doi.org/10.1111/gcb.13673>, 2017.

739 Cox, T. E., Schenone, S., Delille, J., Díaz-Castañeda, V., Alliouane, S., Gattuso, J.-P., and Gazeau, F.: Effects
740 of ocean acidification on *Posidonia oceanica* epiphytic community and shoot productivity, *J. Ecol.*, 103,
741 1594–1609, <https://doi.org/10.1111/1365-2745.12477>, 2015.

742 Dickson, A., Sabine, C. L., and Christian, J. R.: Guide to best practices for ocean CO₂ measurements, PICES
743 Special Publication 3; 191 pp, 2007.

744 Dorey, N., Lançon, P., Thorndyke, M., and Dupont, S.: Assessing physiological tipping point of sea urchin
745 larvae exposed to a broad range of pH, *Glob. Change Biol.*, 19, 3355–3367,
746 <https://doi.org/10.1111/gcb.12276>, 2013.

747 Egilsdottir, H., Noisette, F., Noël, L. M.-L. J., Olafsson, J., and Martin, S.: Effects of pCO₂ on physiology
748 and skeletal mineralogy in a tidal pool coralline alga *Corallina elongata*, *Mar. Biol.*, 160, 2103–2112,
749 <https://doi.org/10.1007/s00227-012-2090-7>, 2013.

750 Foo, S., Byrne, M., Ricevuto, E., and Gambi, M. C.: The carbon dioxide vents of Ischia, Italy, a natural
751 system to assess impacts of ocean acidification on marine ecosystems: An overview of research and
752 comparisons with other vent systems, *Oceanogr. Mar. Biol. Annu. Rev.*, 56, 237–310,
753 <https://doi.org/10.1201/9780429454455-4>, 2018.

754 Ganning, B.: Studies on chemical, physical and biological conditions in swedish rockpool ecosystems,
755 *Ophelia*, 9, 51–105, <https://doi.org/10.1080/00785326.1971.10430090>, 1971.

756 Gao, K. and Beardall, J.: Using macroalgae to address UN Sustainable Development goals through CO₂
757 remediation and improvement of the aquaculture environment, *Appl. Phycol.*, 3, 360–367,
758 <https://doi.org/10.1080/26388081.2022.2025617>, 2022.

759 Gattuso, J.-P., Epitalon, J.-M., Lavigne, H., and Orr, J.: seacarb: seawater carbonate chemistry with R. R
760 package version 3.2.16 <http://CRAN.R-project.org/package=seacarb>, 2021.

761 Gazeau, F., Urbini, L., Cox, T., Alliouane, S., and Gattuso, J.: Comparison of the alkalinity and calcium
762 anomaly techniques to estimate rates of net calcification, *Mar. Ecol. Prog. Ser.*, 527, 1–12,
763 <https://doi.org/10.3354/meps11287>, 2015.

764 Gran, G.: Determination of the equivalence point in potentiometric titrations. Part II, *The Analyst*, 77,
765 661, <https://doi.org/10.1039/an9527700661>, 1952.

766 Haraldsson, C., Anderson, L. G., Hassellöv, M., Hulth, S., and Olsson, K.: Rapid, high-precision
767 potentiometric titration of alkalinity in ocean and sediment pore waters, *Deep Sea Res. Part Oceanogr.*
768 *Res. Pap.*, 44, 2031–2044, [https://doi.org/10.1016/S0967-0637\(97\)00088-5](https://doi.org/10.1016/S0967-0637(97)00088-5), 1997.

769 Houlihan, E. P., Espinel-Velasco, N., Cornwall, C. E., Pilditch, C. A., and Lamare, M. D.: Diffusive boundary
770 layers and ocean acidification: Implications for sea urchin settlement and growth, *Front. Mar. Sci.*, 7,
771 2020.

772 Hurd, C. L., Beardall, J., Comeau, S., Cornwall, C. E., Havenhand, J. N., Munday, P. L., Parker, L. M., Raven,
773 J. A., McGraw, C. M., Hurd, C. L., Beardall, J., Comeau, S., Cornwall, C. E., Havenhand, J. N., Munday, P. L.,
774 Parker, L. M., Raven, J. A., and McGraw, C. M.: Ocean acidification as a multiple driver: how interactions

775 between changing seawater carbonate parameters affect marine life, *Mar. Freshw. Res.*, 71, 263–274,
776 <https://doi.org/10.1071/MF19267>, 2019.

777 IPCC: IPCC Special Report on the Ocean and Cryosphere in a Changing Climate, edited by: Pörtner, H. O.,
778 Roberts, D., Masson-Delmotte, V., and Zhai, P., Cambridge University Press, UK, 755 pp.,
779 <https://doi.org/10.1017/9781009157964>, 2019.

780 Jia, G., E. Shevliakova, P. Artaxo, N. De Noblet-Ducoudré, R. Houghton, J. House, K. Kitajima, C. Lennard,
781 A. Popp, A. Sirin, R. Sukumar, and L. Verchot: Land–climate interactions., in: *Climate Change and Land:*
782 *an IPCC special report on climate change, desertification, land degradation, sustainable land*
783 *management, food security, and greenhouse gas fluxes in terrestrial ecosystems*, 2019.

784 Johnson, M. D., Moriarty, V. W., and Carpenter, R. C.: Acclimatization of the Crustose Coralline Alga
785 *Porolithon onkodes* to Variable pCO₂, *PLOS ONE*, 9, e87678,
786 <https://doi.org/10.1371/journal.pone.0087678>, 2014.

787 Kottmeier, D. M., Chrachri, A., Langer, G., Helliwell, K. E., Wheeler, G. L., and Brownlee, C.: Reduced H⁺
788 channel activity disrupts pH homeostasis and calcification in coccolithophores at low ocean pH, *Proc.*
789 *Natl. Acad. Sci.*, 119, e2118009119, <https://doi.org/10.1073/pnas.2118009119>, 2022.

790 Kroeker, K. J., Micheli, F., and Gambi, M. C.: Ocean acidification causes ecosystem shifts via altered
791 competitive interactions, *Nat. Clim. Change*, 3, 156–159, <https://doi.org/10.1038/nclimate1680>, 2012.

792 Kwiatkowski, L., Gaylord, B., Hill, T., Hosfelt, J., Kroeker, K. J., Nebuchina, Y., Ninokawa, A., Russell, A. D.,
793 Rivest, E. B., Sesboüé, M., and Caldeira, K.: Nighttime dissolution in a temperate coastal ocean
794 ecosystem increases under acidification, *Sci. Rep.*, 6, 22984, <https://doi.org/10.1038/srep22984>, 2016.

795 Kwiatkowski, L., Torres, O., Bopp, L., Aumont, O., Chamberlain, M., Christian, J. R., Dunne, J. P., Gehlen,
796 M., Ilyina, T., John, J. G., Lenton, A., Li, H., Lovenduski, N. S., Orr, J. C., Palmieri, J., Santana-Falcón, Y.,
797 Schwinger, J., Séférian, R., Stock, C. A., Tagliabue, A., Takano, Y., Tjiputra, J., Toyama, K., Tsujino, H.,
798 Watanabe, M., Yamamoto, A., Yool, A., and Ziehn, T.: Twenty-first century ocean warming, acidification,
799 deoxygenation, and upper-ocean nutrient and primary production decline from CMIP6 model
800 projections, *Biogeosciences*, 17, 3439–3470, <https://doi.org/10.5194/bg-17-3439-2020>, 2020.

801 Legrand, E., Riera, P., Pouliquen, L., Bohner, O., Cariou, T., and Martin, S.: Ecological characterization of
802 intertidal rockpools: Seasonal and diurnal monitoring of physico-chemical parameters, *Reg. Stud. Mar.*
803 *Sci.*, 17, 1–10, <https://doi.org/10.1016/j.rsma.2017.11.003>, 2018a.

804 Legrand, E., Riera, P., Bohner, O., Coudret, J., Schlicklin, F., Derrien, M., and Martin, S.: Impact of ocean
805 acidification and warming on the productivity of a rock pool community, *Mar. Environ. Res.*, 136, 78–88,
806 <https://doi.org/10.1016/j.marenvres.2018.02.010>, 2018b.

807 Legrand, E., Riera, P., Lutier, M., Coudret, J., Grall, J., and Martin, S.: Grazers increase the sensitivity of
808 coralline algae to ocean acidification and warming, *J. Sea Res.*, 148–149, 1–7,
809 <https://doi.org/10.1016/j.seares.2019.03.001>, 2019.

810 Lorenzen, S.: The limpet *Patella vulgata* L. at night in air: effective feeding on *Ascophyllum nodosum*
811 monocultures and stranded seaweeds, *J. Molluscan Stud.*, 73, 267–274,
812 <https://doi.org/10.1093/mollus/eym022>, 2007.

813 Mackey, K. R. M., Morris, J. J., Morel, F. M. M., and Kranz, S. A.: Response of photosynthesis to ocean
814 acidification, *Oceanography*, 28, 74–91, 2015.

815 Maneveldt, G. W., Wilby, D., Potgieter, M., and Hendricks, M. G. J.: The role of encrusting coralline algae
816 in the diets of selected intertidal herbivores, *J. Appl. Phycol.*, 18, 619–627,
817 <https://doi.org/10.1007/s10811-006-9059-1>, 2006.

818 Martin, S., Cohu, S., Vignot, C., Zimmerman, G., and Gattuso, J.-P.: One-year experiment on the
819 physiological response of the Mediterranean crustose coralline alga, *Lithophyllum cabiochae*, to
820 elevated $p\text{CO}_2$ and temperature, *Ecol. Evol.*, 3, 676–693, <https://doi.org/10.1002/ece3.475>, 2013a.

821 Martin, S., Charnoz, A., and Gattuso, J.-P.: Photosynthesis, respiration and calcification in the
822 Mediterranean crustose coralline alga *Lithophyllum cabiochae* (Corallinales, Rhodophyta), *Eur. J. Phycol.*,
823 48, 163–172, <https://doi.org/10.1080/09670262.2013.786790>, 2013b.

824 Miller, C. A. and Kelley, A. L.: Alkalinity cycling and carbonate chemistry decoupling in seagrass mystify
825 processes of acidification mitigation, *Sci. Rep.*, 11:13500, <https://doi.org/10.1038/s41598-021-92771-2>,
826 2021.

827 Morris, S. and Taylor, A. C.: Diurnal and seasonal variation in physico-chemical conditions within
828 intertidal rock pools, *Estuar. Coast. Shelf Sci.*, 17, 339–355, [https://doi.org/10.1016/0272-
829 7714\(83\)90026-4](https://doi.org/10.1016/0272-7714(83)90026-4), 1983.

830 Nash, M. C., Diaz-Pulido, G., Harvey, A. S., and Adey, W.: Coralline algal calcification: A morphological
831 and process-based understanding, *PLOS ONE*, 14, e0221396,
832 <https://doi.org/10.1371/journal.pone.0221396>, 2019.

833 Noisette, F., Egilsdottir, H., Davoult, D., and Martin, S.: Physiological responses of three temperate
834 coralline algae from contrasting habitats to near-future ocean acidification, *J. Exp. Mar. Biol. Ecol.*, 448,
835 179–187, <https://doi.org/10.1016/j.jembe.2013.07.006>, 2013.

836 Paiva, F., Brennecke, D., Pansch, C., and Briski, E.: Consistency of aquatic enclosed experiments: The
837 importance of scale and ecological complexity, *Divers. Distrib.*, 27, 524–532, 2021.

838 Pan, T.-C. F., Applebaum, S. L., and Manahan, D. T.: Experimental ocean acidification alters the allocation
839 of metabolic energy, *Proc. Natl. Acad. Sci. U. S. A.*, 112, 4696–701,
840 <https://doi.org/10.1073/pnas.1416967112>, 2015.

841 Pansch, A., Winde, V., Asmus, R., and Asmus, H.: Tidal benthic mesocosms simulating future climate
842 change scenarios in the field of marine ecology, *Limnol. Oceanogr. Methods*, 14, 257–267,
843 <https://doi.org/10.1002/lom3.10086>, 2016.

844 Pinheiro, J., Bates, D., and R-core: Package “nlme”: Linear and Nonlinear Mixed Effects Models, Cran-R,
845 2018.

846 R Core Team: R: A language and environment for statistical computing, 2017.

847 Raven, J. A.: Effects on marine algae of changed seawater chemistry with increasing atmospheric CO_2 ,
848 *Biol. Environ. Proc. R. Ir. Acad.*, 111B, 1–17, 2011.

849 Riebesell, U., Czerny, J., von Bröckel, K., Boxhammer, T., Büdenbender, J., Deckelnick, M., Fischer, M.,
850 Hoffmann, D., Krug, S. A., Lentz, U., Ludwig, A., Mucho, R., and Schulz, K. G.: Technical Note: A mobile
851 sea-going mesocosm system – new opportunities for ocean change research, *Biogeosciences*, 10, 1835–
852 1847, <https://doi.org/10.5194/bg-10-1835-2013>, 2013.

853 Ries, J. B.: Skeletal mineralogy in a high-CO₂ world, *J. Exp. Mar. Biol. Ecol.*, 403, 54–64,
854 <https://doi.org/10.1016/j.jembe.2011.04.006>, 2011.

855 Ries, J. B., Ghazaleh, M. N., Connolly, B., Westfield, I., and Castillo, K. D.: Impacts of seawater saturation
856 state ($\Omega_A=0.4-4.6$) and temperature (10, 25°C) on the dissolution kinetics of whole-shell biogenic
857 carbonates, *Geochim. Cosmochim. Acta*, 192, 318–337, <https://doi.org/10.1016/j.gca.2016.07.001>,
858 2016.

859 Schaal, G. and Grall, J.: Microscale aspects in the diet of the limpet *Patella vulgata* L., *J. Mar. Biol. Assoc.*
860 *U. K.*, 95, 1155–1162, <https://doi.org/10.1017/S0025315415000429>, 2015.

861 Schulz, K. G., Bellerby, R. G. J., Brussaard, C. P. D., Büdenbender, J., Czerny, J., Engel, A., Fischer, M.,
862 Koch-Klavnsen, S., Krug, S. A., Lischka, S., Ludwig, A., Meyerhöfer, M., Nondal, G., Silyakova, A., Stühr, A.,
863 and Riebesell, U.: Temporal biomass dynamics of an Arctic plankton bloom in response to increasing
864 levels of atmospheric carbon dioxide, *Biogeosciences*, 10, 161–180, [https://doi.org/10.5194/bg-10-161-](https://doi.org/10.5194/bg-10-161-2013)
865 2013, 2013.

866 Smith, S. V. and Key, G. S.: Carbon dioxide and metabolism in marine environments, *Limnol. Oceanogr.*,
867 20, 493–495, <https://doi.org/10.4319/lo.1975.20.3.0493>, 1975.

868 Spisla, C., Taucher, J., Bach, L. T., Haunost, M., Boxhammer, T., King, A. L., Jenkins, B. D., Wallace, J. R.,
869 Ludwig, A., Meyer, J., Stange, P., Minutolo, F., Lohbeck, K. T., Nauendorf, A., Kalter, V., Lischka, S., Sswat,
870 M., Dörner, I., Ismar-Rebitz, S. M. H., Aberle, N., Yong, J. C., Bouquet, J.-M., Lechtenböcker, A. K.,
871 Kohnert, P., Krudewig, M., and Riebesell, U.: Extreme levels of ocean acidification restructure the
872 plankton community and biogeochemistry of a temperate coastal ecosystem: A mesocosm study, *Front.*
873 *Mar. Sci.*, 7:611157, 2021.

874 Stumpp, M., Hu, M. Y., Casties, I., Saborowski, R., Bleich, M., Melzner, F., and Dupont, S.: Digestion in sea
875 urchin larvae impaired under ocean acidification, *Nat. Clim. Change*, 3, 1044–1049,
876 <https://doi.org/10.1038/nclimate2028>, 2013.

877 Sulpis, O., Lauvset, S. K., and Hagens, M.: Current estimates of K1* and K2* appear inconsistent with
878 measured CO₂ system parameters in cold oceanic regions, *Ocean Sci.*, 16, 847–862,
879 <https://doi.org/10.5194/os-16-847-2020>, 2020.

880 Sulpis, O., Jeansson, E., Dinauer, A., Lauvset, S. K., and Middelburg, J. J.: Calcium carbonate dissolution
881 patterns in the ocean, *Nat. Geosci.*, 14, 423–428, <https://doi.org/10.1038/s41561-021-00743-y>, 2021.

882 Torres, O., Kwiatkowski, L., Sutton, A. J., Dorey, N., and Orr, J. C.: Characterizing mean and extreme
883 diurnal variability of ocean CO₂ system variables across marine environments, *Geophys. Res. Lett.*, 48,
884 e2020GL090228, <https://doi.org/10.1029/2020GL090228>, 2021.

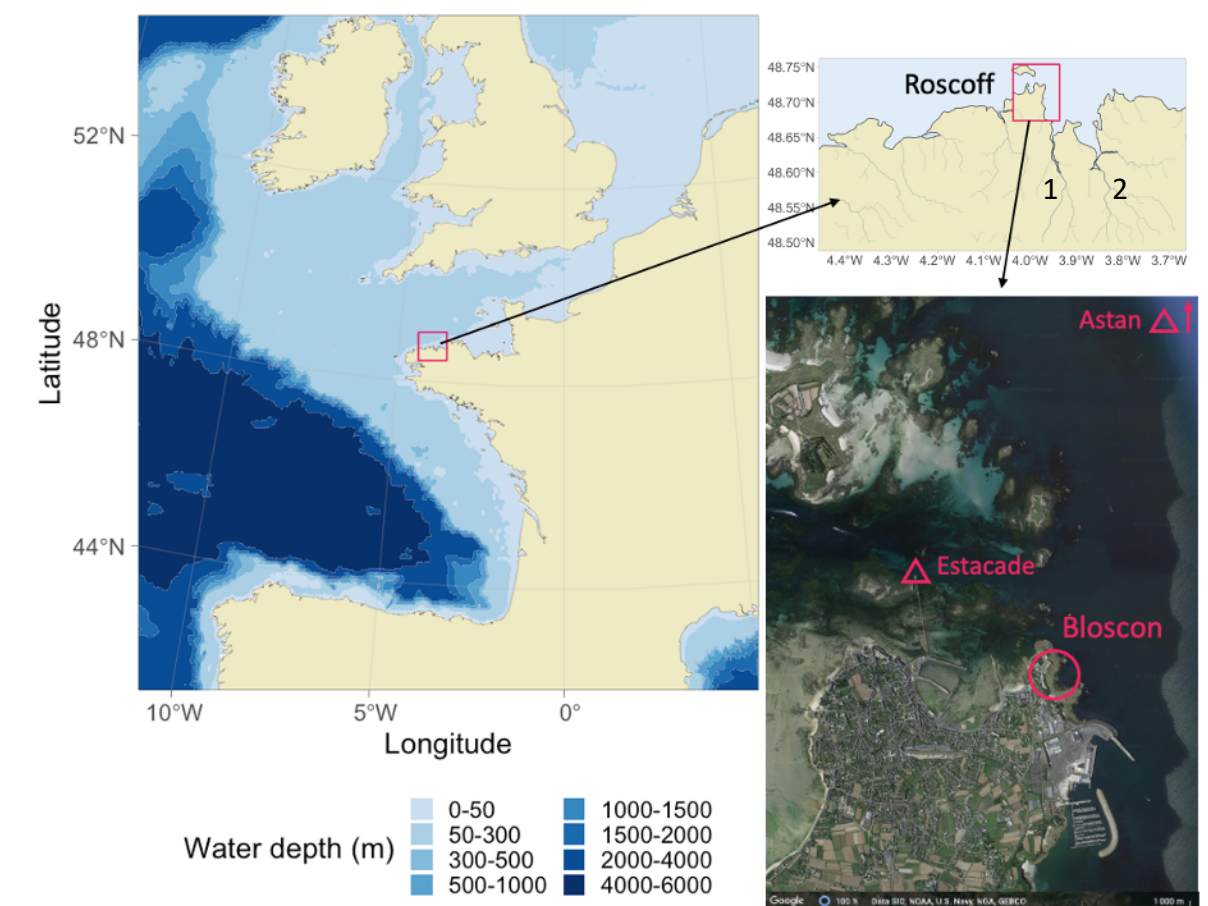
885 Widdicombe, S., Dupont, S., and Thorndyke, M.: Laboratory experiments and benthic mesocosm studies,
886 in: Guide to best practices for ocean acidification research and data reporting. U. Riebesell, V. J. Fabry, L.
887 Hansson and J.-P. Gattuso., Publications Office of the European Union, Luxembourg, 2010.

888 Williamson, C. J., Perkins, R., Voller, M., Yallop, M. L., and Brodie, J.: The regulation of coralline algal
889 physiology, an in situ study of *Corallina officinalis* (Corallinales, Rhodophyta), *Biogeosciences*, 14, 4485–
890 4498, <https://doi.org/10.5194/bg-14-4485-2017>, 2017.

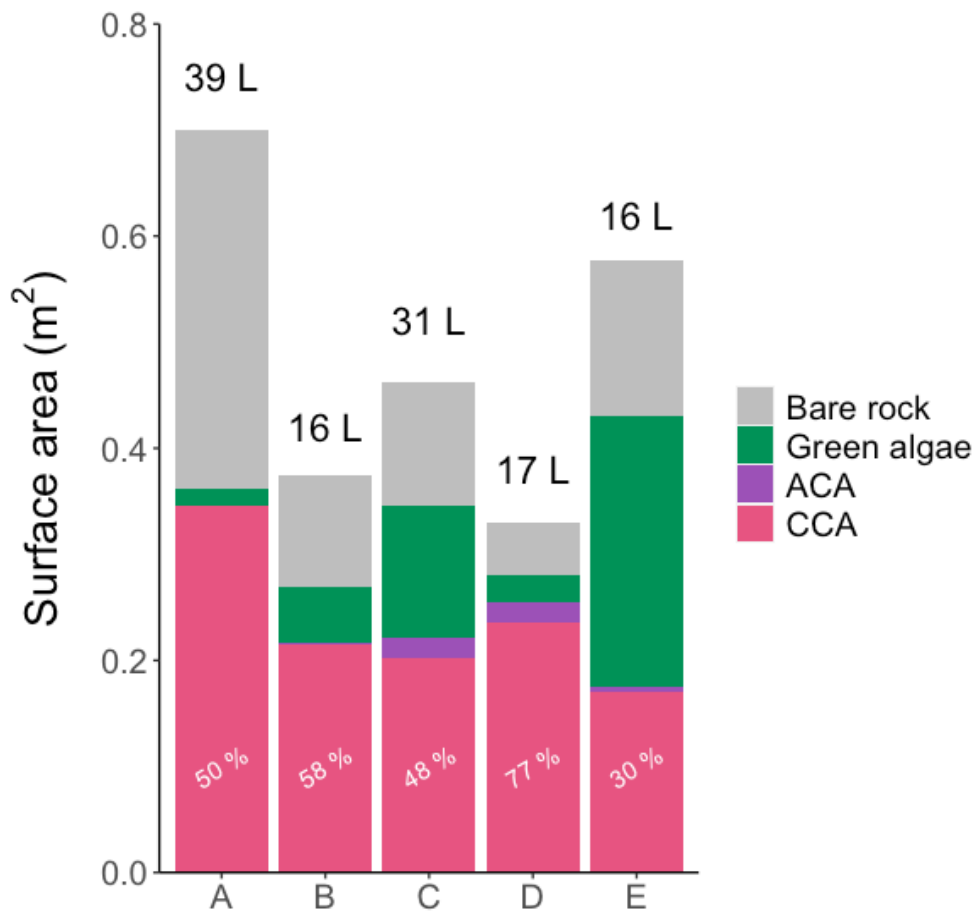
891 Yamamoto, S., Kayanne, H., Terai, M., Watanabe, A., Kato, K., Negishi, A., and Nozaki, K.: Threshold of
892 carbonate saturation state determined by CO₂ control experiment, *Biogeosciences*, 9, 1441–1450,
893 <https://doi.org/10.5194/bg-9-1441-2012>, 2012.

894

1 Figures with legends -

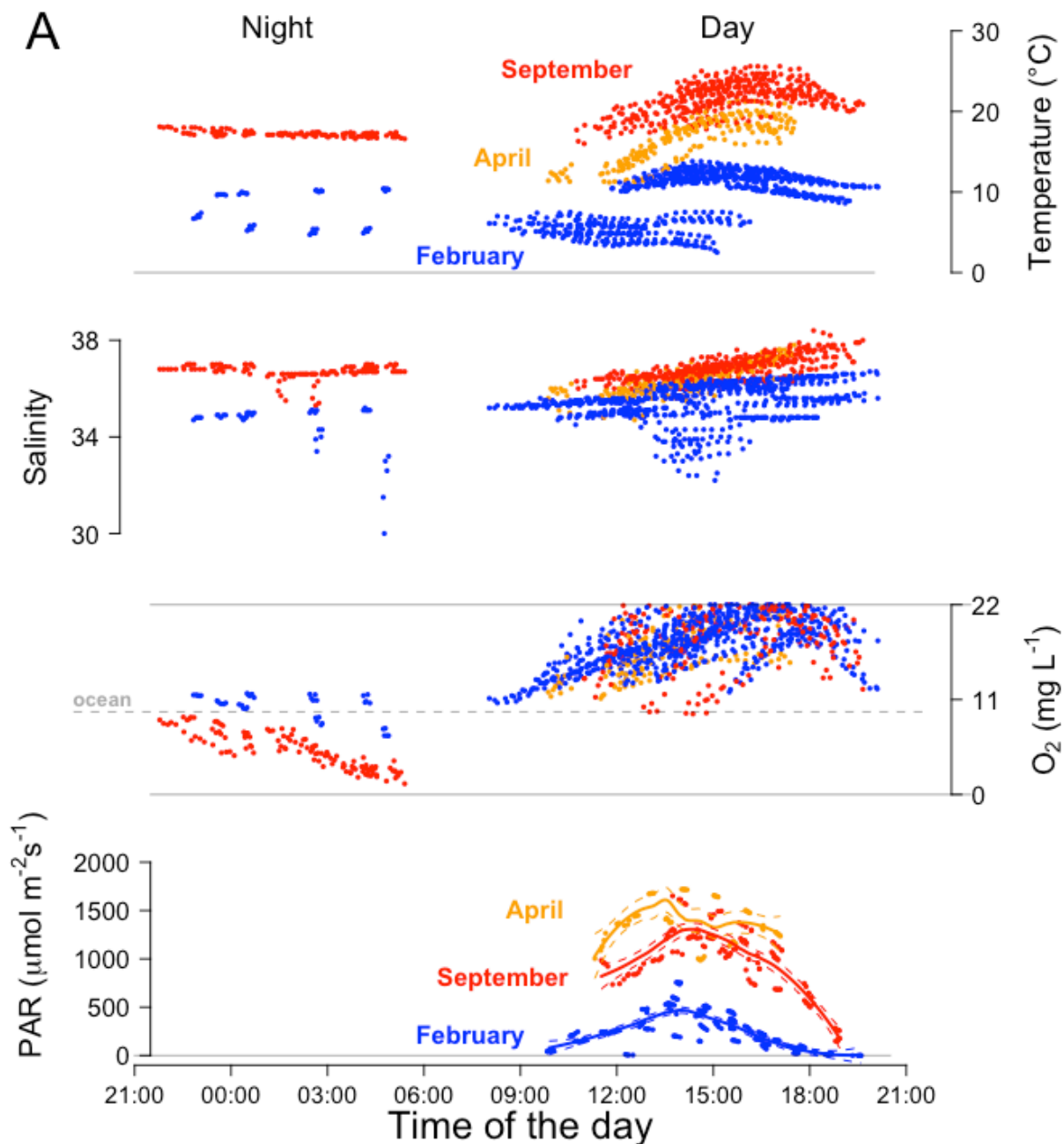


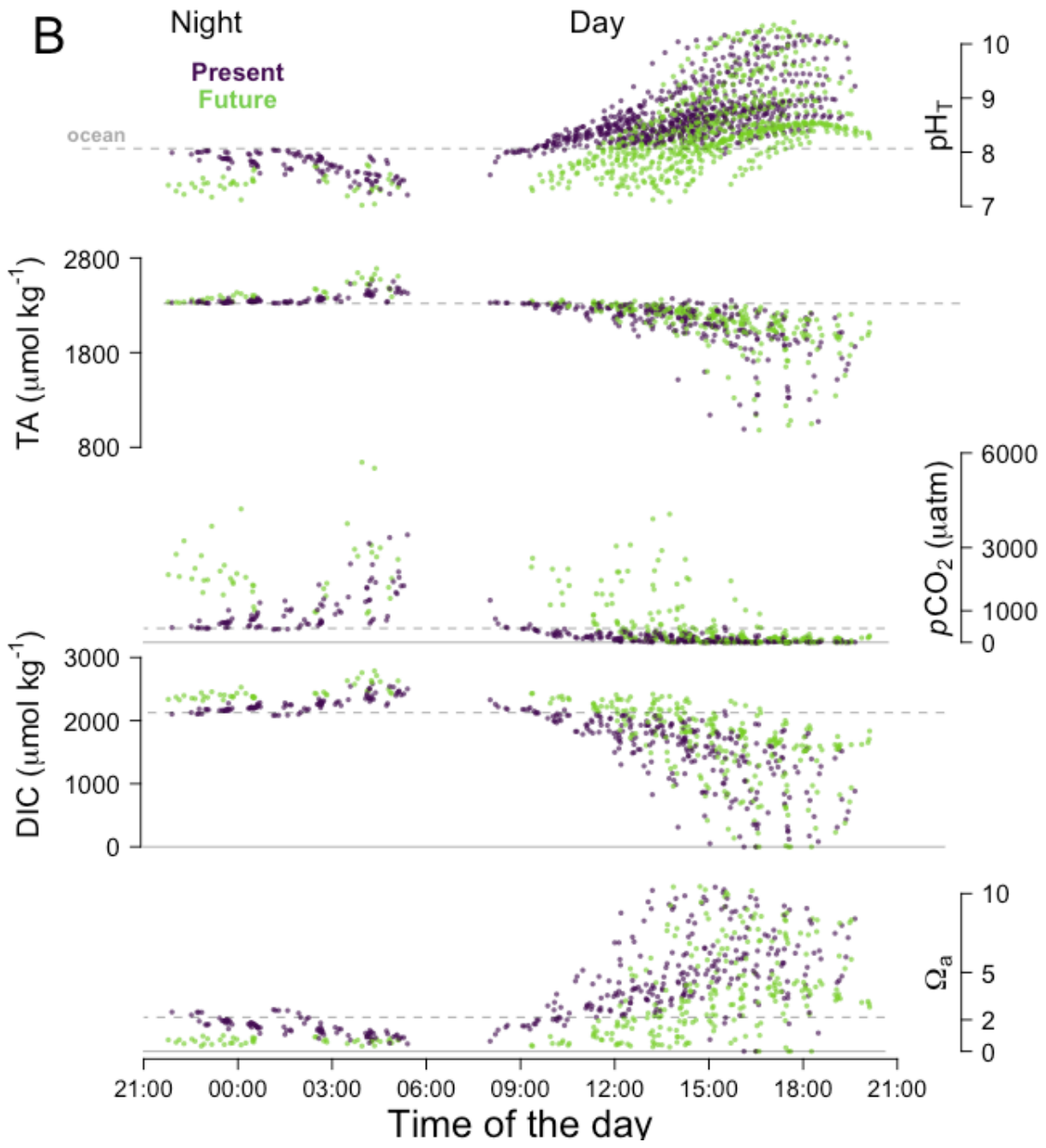
2 **Figure 1 - Field site location** on a map of Europe (left). The study site (Bloscon) is located in
3 Roscoff, Brittany, France (right, top: river mapping data from *HydroSHEDS*, 1. Penzé river and 2.
4 Morlaix river; bottom: satellite image from © Google Earth: earth.google.com/web/, acquired in June
5 2022). The SOMLIT stations Astan and Estacade are indicated with triangles (www.somlit.fr).

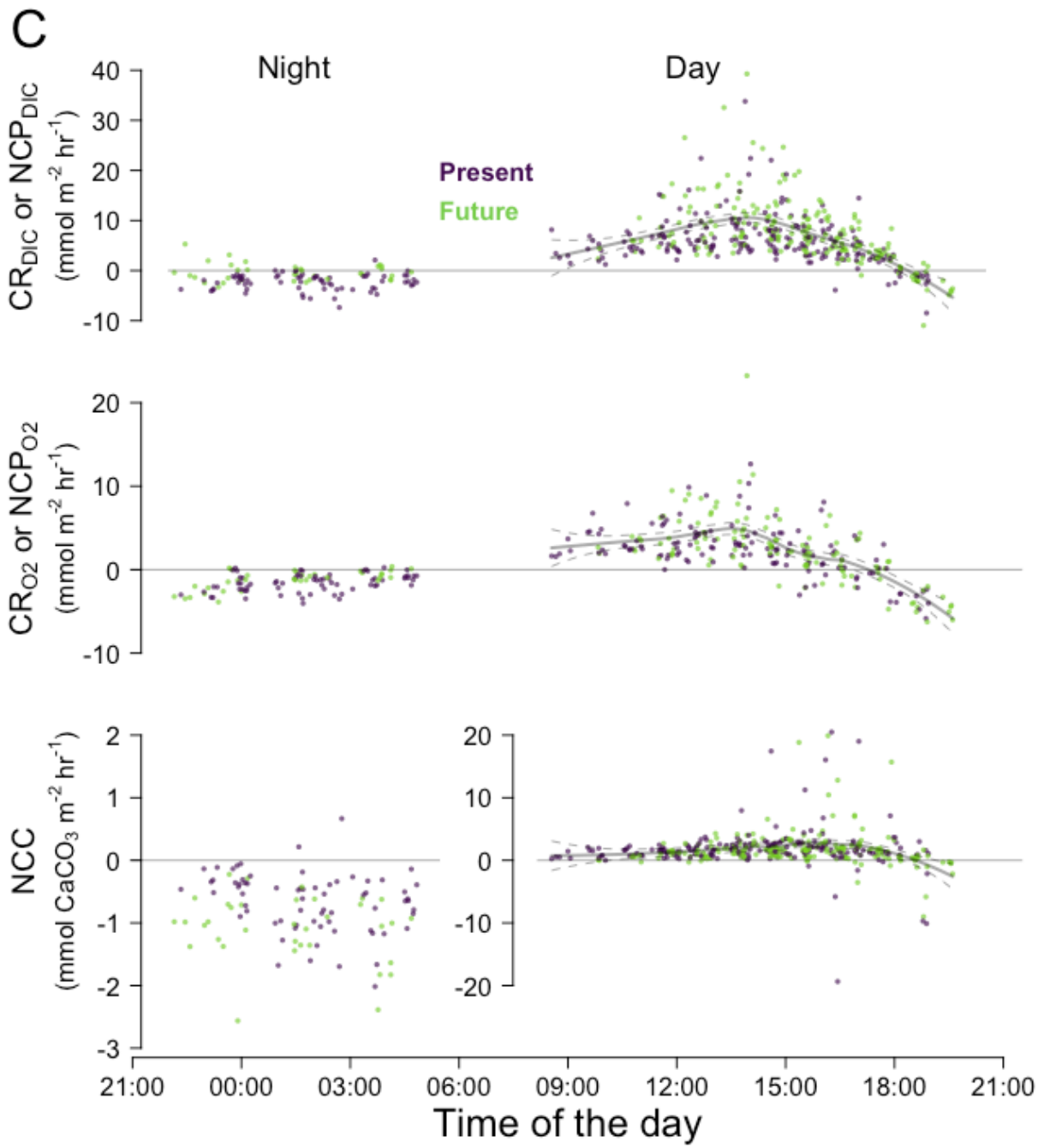


7 **Figure 2 - Pool area, volume and coverage** - Surface of the five pools (A-E, September 2020) covered
8 by crustose coralline algae (CCA, pink), articulated coralline algae (ACA, purple) and green algae
9 (green) or free of algae (“bare rock”, grey). The length of the bars represents total pool surface area
10 (m²) and the volume of each pool (L) is indicated above. The relative coverage (%) of calcifying algae
11 (ACA + CCA) in each pool is given. Details for the other seasons are available in **Supp. Mat. Pools**
12 **Fig. SP1 and SP2.**

13 **Figure 3** - Composite daily pool conditions and biological activity for all pools. A) temperature
 14 ($^{\circ}\text{C}$), salinity and oxygen concentration (mg L^{-1}) and Photosynthetically Active Radiation (PAR,
 15 $\mu\text{mol m}^{-2} \text{s}^{-1}$), B) pH_T , Total Alkalinity (TA, $\mu\text{mol kg}^{-1}$), pCO_2 (μatm), dissolved inorganic carbon
 16 (DIC, $\mu\text{mol kg}^{-1}$) and aragonite saturation state (Ω_a), and C) DIC and O_2 -derived NCP or CR
 17 ($\text{mmol C or O m}^{-2} \text{hr}^{-1}$) and NCC ($\text{mmol CaCO}_3 \text{ m}^{-2} \text{hr}^{-1}$). Colors represent seasons (A: blue for
 18 February, orange for April, red for September) and treatment (B and C: purple for “present” and green
 19 for “future”). Horizontal dotted grey lines represent the mean values of the adjacent ocean. Curves
 20 were fitted by season for PAR and for diurnal NCP and NCC using a local polynomial regression
 21 (*loess*) with 95% confidence interval. Number of observations: $n = 1551$ for temperature, salinity and
 22 pH_T , $n = 1169$ for oxygen concentration (data recorded $< 22 \text{ mg L}^{-1}$) and $n = 632$ (hourly data) for the
 23 carbonate chemistry parameters, NCC and NCP or CR (B). All pools are shown.



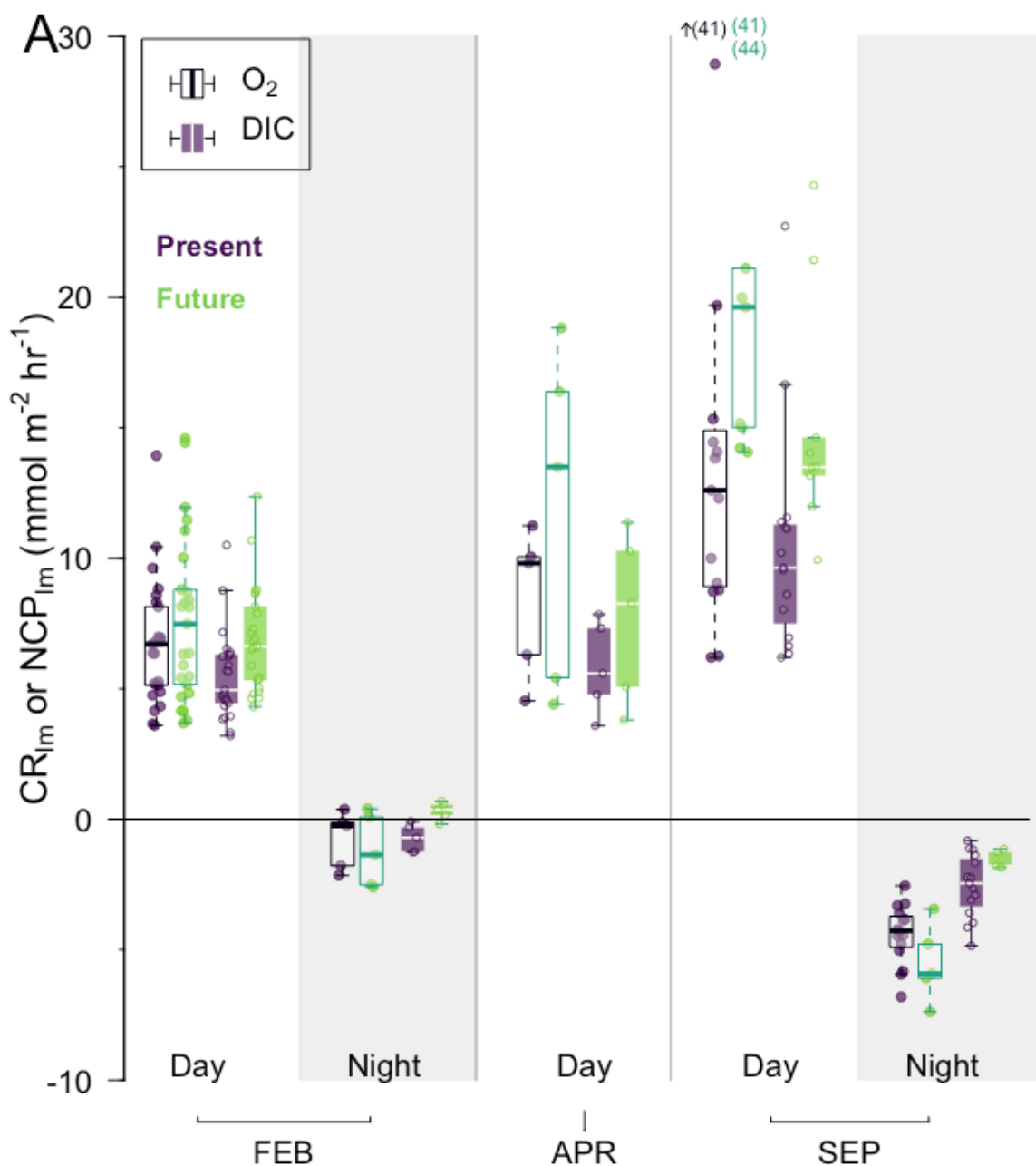




26

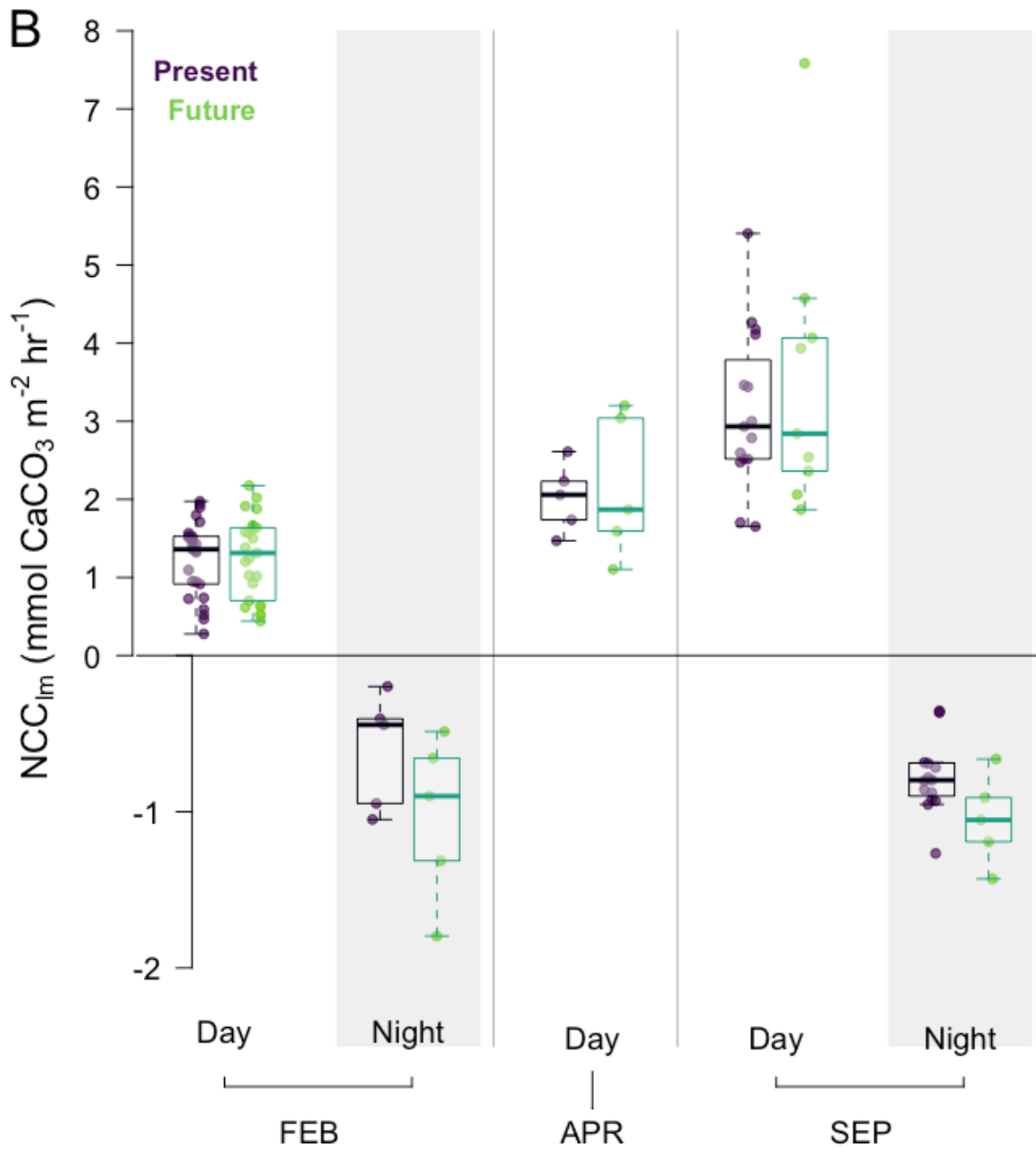
27

28 **Figure 4 – A) O₂-derived (white boxes) and DIC-derived (colored boxes) NCP_{lm} (mmol m⁻² hr⁻¹),**
 29 **and B) NCC_{lm} (mmol CaCO₃ m⁻² hr⁻¹) during the day and night (shaded areas), by season and**
 30 **by treatment** (purple for “present” and green for “future”) – Rates are presented as boxplots showing
 31 median, 1st and 3rd quartile and 1.5 inter-quartile range (bars), with overlaid individual observations
 32 (round symbols). Individual rates were calculated for each pool, each tide and each treatment: n = 50
 33 (FEB-day), n = 10 (FEB-night), n = 10 (APR-Day), n = 25 (SEP-Day), n = 20 (SEP-Night). Seasons:
 34 FEB for winter (pooled February 2020 and 2021), APR for spring (April 2021) and SEP for summer
 35 (pooled September 2020 and 2021). *Note that for NCC_{lm}, nights (<0) and days (>0) have different y-*
 36 *axis scales for better visualization of night differences. Statistical details of the linear regressions can*
 37 *be found in the corresponding **Supplementary Materials**. For O₂-derived NCP_{lm}, in September, three*
 38 *rates were out of the range plotted and their values are indicated next to the small arrow.*



39

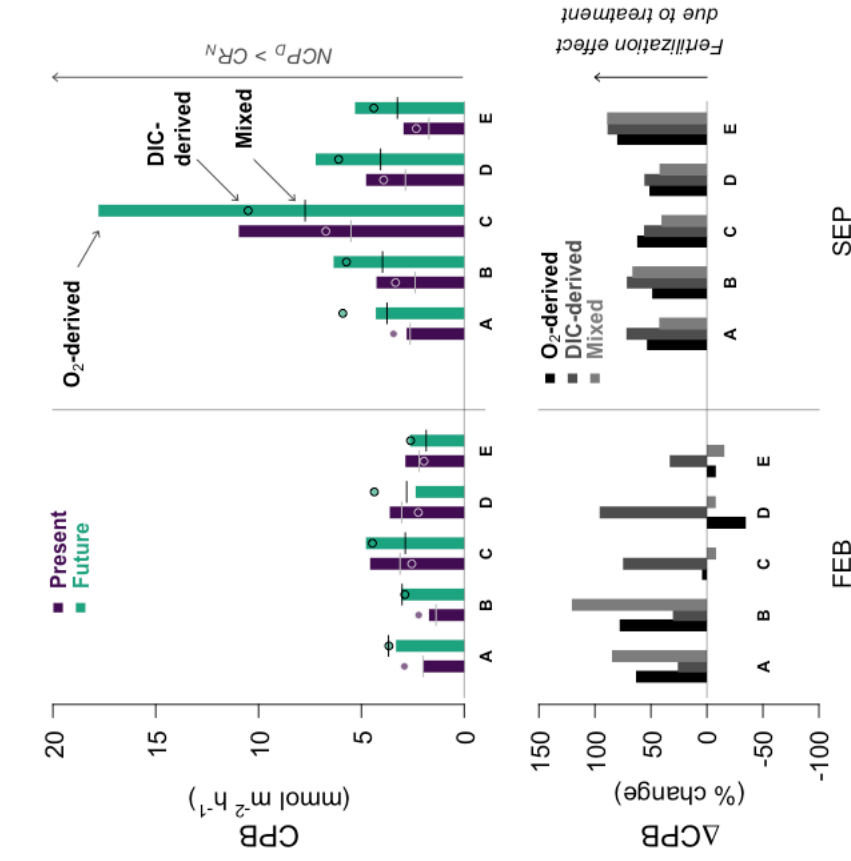
40



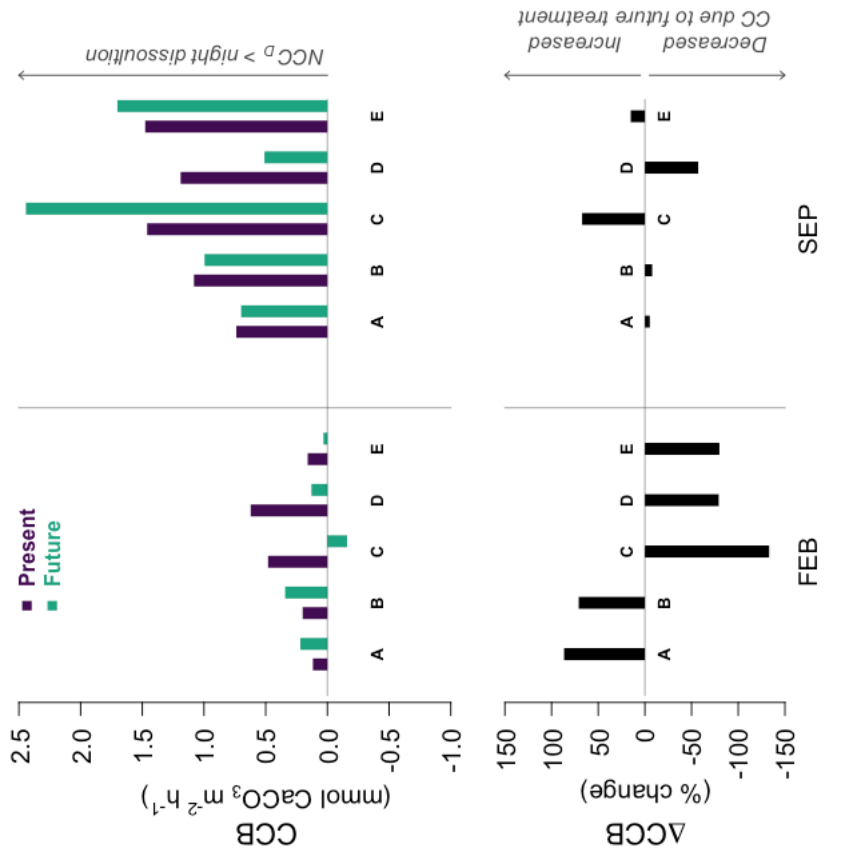
41

42

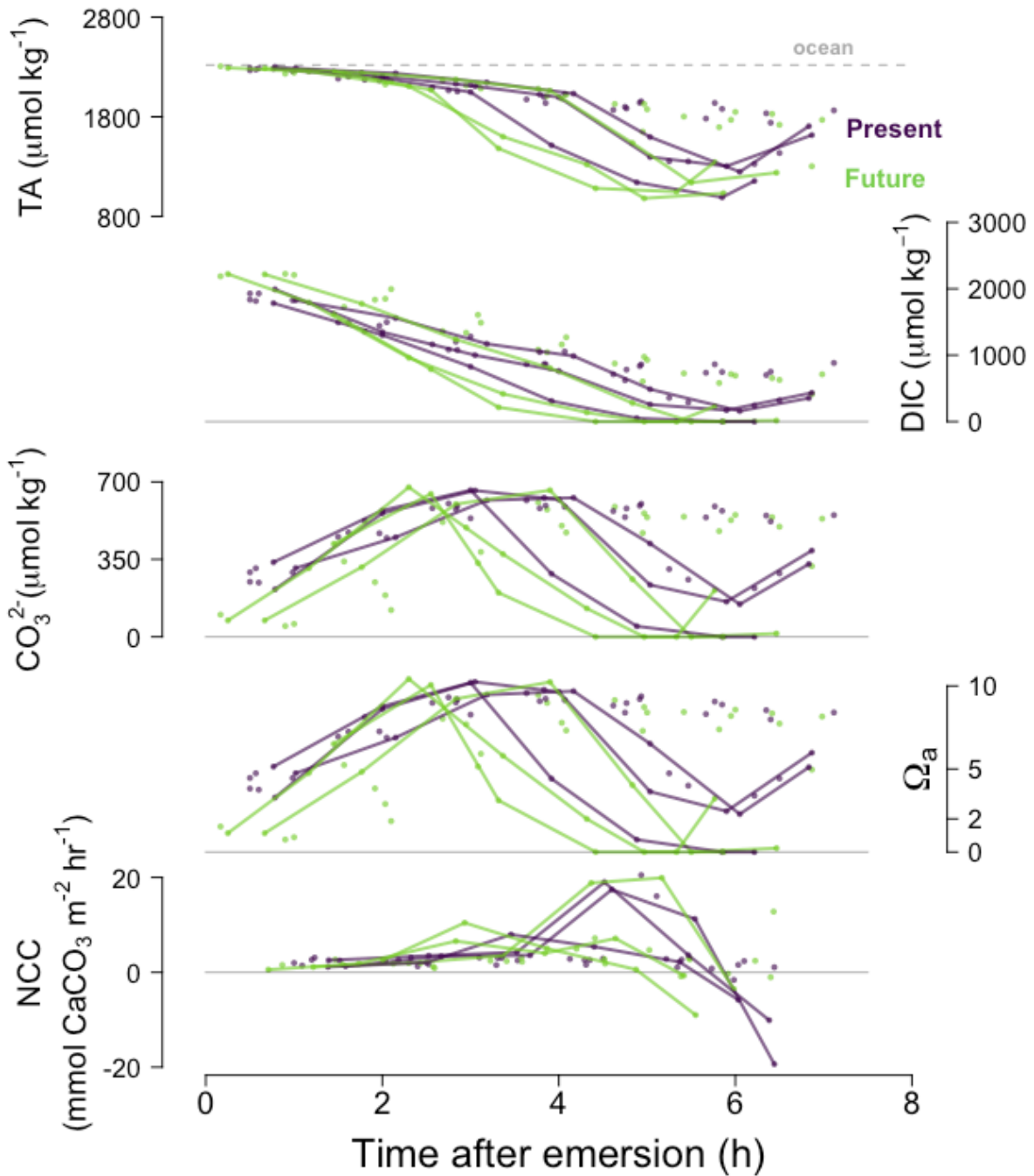
Community production budget



Community calcification budget



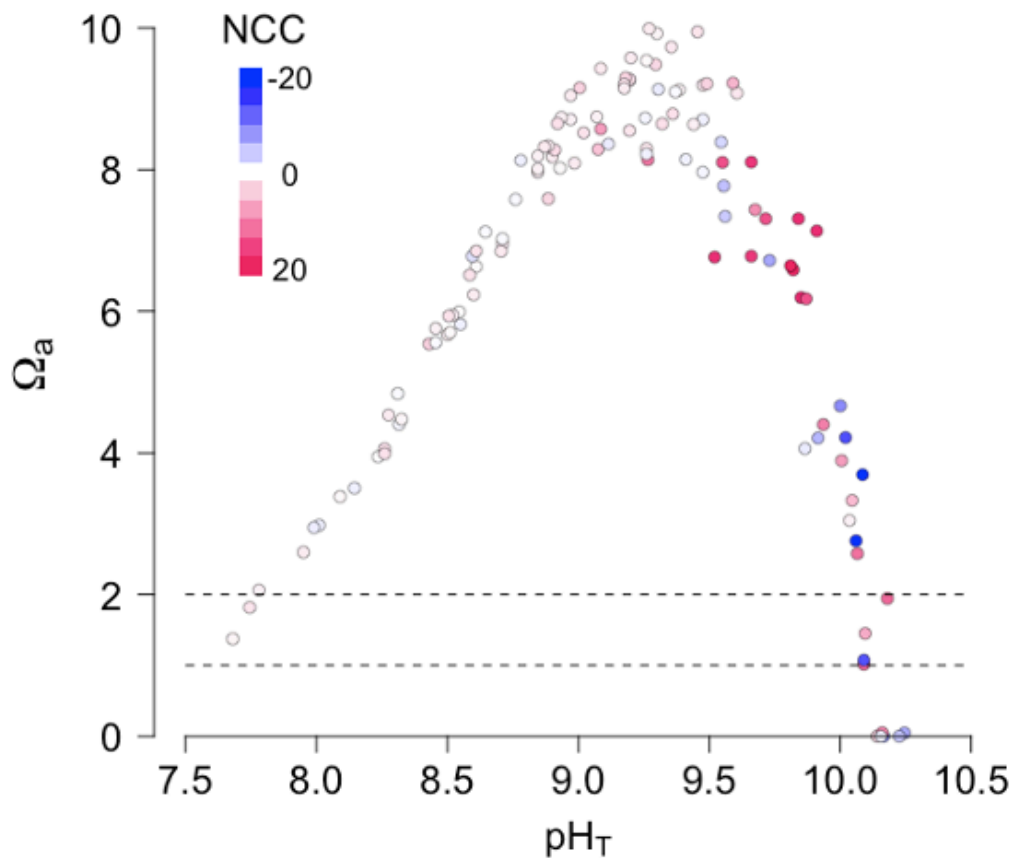
43 **Figure 5 – Community production budget: CPB¹⁾, and calcification budget: CCB (upper right panel, mmol CaCO₃ m⁻² hr⁻¹) by treatment**
 44 (purple for “present” and green for “future”) for each pool and season (same legend as Fig. 4). CPB >0 if diurnal NCP > nocturnal respiration and
 45 CCB > 0 if diurnal NCC > nocturnal dissolution. CPB was estimated three different ways: from O₂-derived NCP (bars), from DIC-derived NCP
 46 (round symbols) and from nocturnal O₂-derived CR combined with diurnal DIC-derived NCP (“mixed”, vertical segments). **The bottom panels**
 47 **present the change (%) of diel production (ΔCPB: left) and diel calcification (ΔCCB: right) due to CO₂ addition.** Positive ΔCCB indicates
 48 a fertilization effect due to the CO₂ addition; negative ΔCCB is expected if the CO₂ addition decreases net calcification/increases net dissolution.
 49 All three methods to estimate CPB indicate a fertilization effect in summer.



50

51 **Figure 6 - Time series for September 2020 diurnal data only: A) Total Alkalinity (TA, $\mu\text{mol kg}^{-1}$),**
 52 **dissolved inorganic carbon, CO_3^{2-} concentration ($\mu\text{mol kg}^{-1}$), aragonite saturation state (Ω_a)**
 53 **and NCC ($\text{mmol m}^{-2} \text{hr}^{-1}$) with time after emersion, by treatment (purple for “present” and green**
 54 **for “future”). The lines in bold represent individual pools C and E that switched from calcification to**
 55 **dissolution when pH_T was still above 9. A similar figure in **Supp. Mat. (Fig. S4)** shows that**
 56 **sunset/irradiance are not correlated with the sudden change towards dissolution.**

57



58 **Figure 7 – At very high pH there was both fast net calcification (red) and rapid net dissolution**
 59 **(blue):** In some extreme cases, pH_T was not a good indicator of seawater saturation state (Ω_a). Selected
 60 dataset of diurnal low-tide emersion periods from September 2020. Colors represent NCC (in mmol
 61 $\text{CaCO}_3 \text{ m}^{-2} \text{ hr}^{-1}$, as presented in **Fig. 3C**). Dashed horizontal lines represent saturation state for
 62 aragonite ($\Omega_a = 1$) and for high-Mg calcite ($\Omega_a = 2$).